

Technical Report No. 11-1554E-76-6

AC
2

ADA 024855

See
1473

**INVESTIGATION
OF
FINITE AMPLITUDE ATTENUATION**

Final Report
30 April 1976

Prepared Under Contract N00039-75-C-0263
ARPA Order No. 2910, Program Code 5G10
for

THE NAVAL SEA SYSTEMS COMMAND

J. C. LOCKWOOD

RECEIVED
MAY 26 1976
D. R. C.

Approved for Public Release; Distribution Unlimited

AMETEK

STRAZA DIVISION • 790 GREENFIELD DRIVE, EL CAJON, CA 92021

INVESTIGATION OF FINITE AMPLITUDE ATTENUATION
FINAL TECHNICAL REPORT
29 February 1976

James C. Lockwood

NAVAL ELECTRONICS SYSTEMS COMMAND
Contract N00039-75-C-0263
ARPA Order 2910, Program Code 5G10

Sponsored by
Advanced Research Projects Agency
ARPA Order No. 2910

Effective Date of Contract, 29 March 1975
Expiration Date of Contract, 31 December 1975
Amount of Contract, \$54,101.60

The views and conclusions contained in this document are those of the author and should not be interpreted as necessarily representing the official policies, either expressed or implied, of the Advanced Research Projects Agency or the United States Government.

AMETEK, Straza Division
790 Greenfield Drive
El Cajon, California 92022
(714) 442-3451

D. D. S.
RECEIVED
MAY 28 1976
C

SEARCHED	INDEXED	SERIALIZED	FILED
<input type="checkbox"/>	<input type="checkbox"/>	<input type="checkbox"/>	<input type="checkbox"/>
MAY 28 1976			
FBI - EL CAJON			

SUMMARY

This is the final technical report on a study of finite amplitude attenuation that has been performed under Contract N00039-75-C-0263, Program Code 5G10, ARPA Order 2910. The program objective has been to determine by experimental and theoretical means the limitations imposed by finite amplitude attenuation on the performance of parametric sonars. The results are intended for use in assessing the potential of parametric receivers and transmitters in military applications.

The axial response of the parametric receiving array has been calculated in two ways. The first is by use of a one dimensional model in which the secondary signal levels are predicted from weak shock theory. The second is by numerical evaluation of the scattering integral solution in which finite amplitude attenuation is introduced by means of a taper function derived from the one dimensional solution.

An experiment has been performed in which the axial secondary signal level as a function of pump source level was measured. These data agree with the theoretical results, but the agreement is not conclusive because the maximum pump source level was not sufficiently high. However, a comparison with data from another investigation confirms the theory for cases when the receiving hydrophone is well in the farfield of the pump.

Comparison with a set of experimental results for which the interaction was almost entirely in the pump nearfield indicates that, unlike the farfield case, the nearfield behavior may be quite different from that predicted by the present theory. Caution is therefore advised in applying the present results to nearfield interactions.

In addition to the parametric receiving array work, several parametric transmitting array taper functions have been compared in the context of numerical evaluations of the scattering integral. A mean taper function is derived from weak shock theory and is compared with the others.

In all cases the results are surprisingly similar to those obtained using the model given by Mellen and Moffett.

TABLE OF CONTENTS

<u>Section</u>	<u>Title</u>	<u>Page</u>
	SUMMARY	i
	LIST OF SYMBOLS	iv
1.0	INTRODUCTION	1
1.1	Background	3
2.0	PARAMETRIC RECEIVING ARRAY AXIAL RESPONSE	6
2.1	Weak Shock Theory Formulation of Parametric Receiving Array Axial Response	7
2.2	Scattering Integral Evaluation of Parametric Receiving Array Axial Response	14
2.3	Comparison of Theoretical Results with Experimental Data of Other Investigators	21
2.4	Experimental Measurement of Parametric Receiver Amplitude Response	28
2.5	Conclusions: Parametric Receiving Array Finite Amplitude Taper	33
3.0	TAPER FUNCTIONS AND THE PARAMETRIC TRANSMITTING ARRAY	35
3.1	Derivation of the Intensity Taper Function	36
3.2	Numerical Results - Phase Reversed Parametric Array	39
3.3	Comparison of Various Taper Functions	40
3.4	Comparison of Parametric Transmitting Array Calculations using Various Taper Functions	45
3.5	Conclusions: Parametric Transmitting Array Finite Amplitude Effects	48
4.0	RECOMMENDATIONS FOR FUTURE WORK	49
5.0	ACKNOWLEDGEMENTS	50
	REFERENCES	51

LIST OF SYMBOLS

a	-	Piston radius
B_n	-	Harmonic coefficient (Fourier sine series)
B_1'	-	First derivative of B_1 with respect to its argument
c_o	-	Small signal sound speed
$D(\theta)$	-	Directivity function
i	-	$\sqrt{-1}$
I	-	Intensity
$J_n(\cdot)$	-	Bessel function of order n
k_o	-	Pump frequency wave number ω_o/c_o
k_{\pm}	-	Secondary frequency wave number
k_s	-	Signal frequency wave number
L	-	Distance from signal source to pump
P_o	-	Pump acoustic pressure at range R_o
P_{\pm}	-	Acoustic pressure at sum (+) or difference (-) frequency
P_s	-	Signal acoustic pressure at receiver
p	-	Composite pressure signal
r	-	Range
r'	-	Dummy variable of integration
r_o	-	Effective source radius
R_o	-	Rayleigh distance (area/ λ)
y	-	Retarded time
α_o	-	Absorption coefficient at pump frequency; absorption coefficient at mean primary frequency.

α_s	-	Absorption coefficient at signal frequency
α_T	-	Sum of absorption coefficients at two primary frequencies
α_{\pm}	-	Absorption coefficient at secondary frequency
β	-	Nonlinearity coefficient ($1 + B/2A \doteq 3.5$ for water)
δ_0	-	Ratio of signal amplitude to pump amplitude at r_0
$\delta(r)$	-	Ratio of signal amplitude to pump amplitude at range r
ϵ	-	Peak particle velocity Mach number
ϕ	-	Azimuth angle coordinate; also phase.
ϕ_{∞}	-	Angular location of first null of beam pattern
λ	-	Wavelength
ρ_0	-	Static density of medium
$\sigma; \sigma_s$	-	Distortion parameters
σ_0	-	$\beta \epsilon k r_0$
Ω	-	ω_s / ω_0
ω_{\pm}	-	Angular sum or difference frequency
ω_0	-	Pump angular frequency
ω_s	-	Angular frequency of signal
ω_d	-	Difference angular frequency
ω_c	-	Carrier angular frequency

1.0 INTRODUCTION

This is the Final Technical Report under Contract N00039-75-C-0263, Program Code 5G10, ARPA Order 2910. The program objective has been to determine, by experimental and theoretical means, the limitations imposed by finite amplitude attenuation on the performance of parametric sonar. The main emphasis in this work has been on the parametric receiving array which, in contrast to the parametric transmitting array, has received only a small amount of previous attention so far as finite amplitude attenuation is concerned.

The axial response of the parametric receiving array has been modeled in two ways. The first model consists of a one dimensional wave undergoing time domain distortion to produce sum and difference frequencies as it propagates from the pump projector to the receiving hydrophone. In the second model, the parametric receiver is represented as a volume source of sum and difference frequencies that scatter from each point in the interaction volume and are summed at the receiving hydrophone. In the latter model the finite amplitude attenuation is introduced by means of a taper function derived from the one dimensional model.

With the introduction of a simple correction to the one dimensional model to account for nearfield diffraction effects, the two models agree quite well with each other. The experimental results for cases when the receiving hydrophone is well in the farfield of the pump are also in close agreement with the theory. There is, however, evidence that the taper model used may not be adequate for describing the effects of finite amplitude attenuation in the nearfield of the pump. There, the loss due to saturation (based on the only available set of experimental data) appears to be considerably less than expected. This agrees with the results of an alternative taper function that is simply equal to the fundamental component amplitude in the saturating pump signal.

The taper function derived herein is based on farfield considerations and is believed to be realistic. While it is tempting, based on the

apparently different behavior in the nearfield to combine the two types of taper, this has not been done owing to the lack of theoretical justification and the availability of only a single source of nearfield data. Thus, application of the theory presented here for the axial response of the parametric receiving array should be restricted to cases in which the receiving hydrophone is well in the farfield of the pump.

The experimental portion of this investigation produced data for the axial response of the parametric receiving array that agrees well with the theory as calculated by the methods described herein. However, efforts to produce a pump signal of sufficient intensity to make the results regarding the effects of saturation conclusive were unsuccessful. It has, therefore, been necessary to rely on results obtained by other investigators for validation of the theory.

As a secondary task of the present investigation the parametric transmitting array was modeled by use of numerical evaluation of the volume scattering integral with inclusion of a taper function capable of accounting for finite amplitude attenuation as a function of source amplitude, range and angle relative to the acoustic axis of the projector. The model was so constructed that a variety of taper functions could be used for comparison purposes in addition to the one derived in this report. Several such taper functions are compared both as to their mathematical form and as to their performance in the scattering integral evaluation. The performance of the model with the taper function derived in this report is tested by comparison of computed results with experimental data obtained by Mellenbruch and Muir¹ for the case of a parametric array reflected from a pressure release surface a short distance from the projector.

The technical body of this report is organized into two major sections following the introductory material in Section 1.0. Section 2.0 contains the treatment of the parametric receiving array including theory, experiment, comparison with available data and conclusions. Section 3.0 deals with finite amplitude effects in parametric transmitting arrays.

The technical body is now preceded by a brief review of the background of the parametric array.

1.1 Background

The parametric array had its beginnings about 1960 with the theoretical work of Westervelt.^{2,3} Westervelt's analysis showed that if a sound wave consisting of two discrete high frequencies could be confined to a narrow, collimated beam, the two components would interact to produce a sound wave at the difference frequency. This is the basis of the parametric transmitting array. He showed that the directivity of the difference frequency sound wave far from the interaction region, would depend only on the attenuation at the primary frequencies and on the difference frequency wave number. The interaction region is limited by the attenuation at the primary frequencies.

In addition to the assumption that the primary beam acted as a line source, Westervelt assumed that the primary wave attenuation was adequately described by linear theory (i. e., that the amplitude was not so high that finite amplitude attenuation became a factor). Early experimental results confirming Westervelt's theory were published by Bellin and Beyer.⁴ Westervelt also observed that a high frequency pump could be made to function as a receiver by nonlinear interaction with a low frequency signal. This is the basis of the parametric receiving array.

Numerous authors have extended the basic parametric transmitting and receiving array theories to describe more realistic geometries and to account for high amplitudes. There have been two basic approaches to handling geometry. The first is to approximate the interacting signals as one dimensional propagating waves (see, for example, Refs. 5 and 6). The second is to perform a three dimensional integration as was done by Muir and Willette.⁷ The latter approach is the more general but is less amenable to extension to account for finite amplitude effects. It has, in fact, been the former approach that has been used almost exclusively in dealing with finite amplitude effects.

Very little work has been done in analyzing finite amplitude effects in parametric receiving arrays. Experimental data showing saturation in parametric receivers have been published by Berktaf and Al-Temimi⁸ and by Konrad, Mellen and Moffett.⁹ A theoretical model was presented by Bartram¹⁰ for cases when both pump and signal are plane waves. Other geometries have not been dealt with.

Other work related to the parametric receiving array has been done by Fenlon¹¹ in addressing a multiple frequency parametric source. Schaffer and Blackstock¹² also performed related work in their study of modulation of an intense high frequency signal by a low frequency signal.

Finite amplitude effects in parametric transmitting arrays have been dealt with by Mellen and Moffett,¹³ Merklinger,¹⁴ Bartram and Westervelt,¹⁵ and Fenlon.^{16, 17} In all cases, quasi one dimensional models were utilized although Merklinger did formulate the problem in more generality.

The treatment of finite amplitude attenuation in parametric arrays is generally based on one dimensional models and often on theories originally formulated for single frequency sources. Useful theoretical treatments of single frequency sources have been given by Blackstock.^{18, 19} A numerical solution for spherical waves of arbitrary spectrum has been given by Fenlon.²⁰ Single frequency waves from piston sources have been studied by Merklinger, Berktaf and Safar,²¹ Shooter, Muir and Blackstock,²² Lockwood,^{23, 24} Lockwood, Muir and Blackstock,²⁵ and Browning and Mellen.²⁶

Experimental data that demonstrate the performance of various experimental parametric transmitters have been reported by Muir and Willette,⁷ Muir and Blue,²⁷ Merklinger,¹⁴ and numerous others. One specific experiment that is quite valuable for verifying the detailed behavior of a parametric transmitting array theory is the phase reversed parametric array experiment reported by Mellenbruck and Muir.¹ There a parametric array was reflected from a pressure release surface at a range of four yards. The reflection caused a return of energy from the harmonics to the fundamental component of the carrier signal, thereby supposedly prolonging the interaction and increasing the efficiency. The expected efficiency increase was never measured.

A theoretical attempt by Lockwood²⁸ at describing the phase reversed array disclosed a weakness in the concept on which the model used was based and led to the development of the taper function model described in Section 3.1 of the present report.

PARAMETRIC RECEIVING ARRAY AXIAL RESPONSE

The prediction of finite amplitude behavior in the parametric receiving array is, in the present work, based on analysis of the time domain distortion of a composite wave that initially consists of an intense, monochromatic pump wave and a low amplitude signal wave. As the composite wave travels, distortion components are produced by the modulation of the pump wave by the signal wave and of the signal wave by the pump wave, the latter being generally a small effect.

The distortion components of interest, i. e., sum and difference frequencies, are generally close in frequency to the pump signal, and in the pump farfield they travel with the pump wave. On the other hand, distortion signals produced in the pump nearfield are subject to diffraction. It is because of these nearfield generated signals that a purely one dimensional model does not, in general, adequately describe the axial response of the parametric receiver.

The geometric spreading of the secondary signals is handled by two different methods. First, the one dimensional model derived in Section 2.1 is corrected, as described in Section 2.1.1, by a simple geometrical factor that approximately compensates for diffraction in the nearfield. Then in Section 2.2 a second model is described wherein the geometry is dealt with rigorously using the scattering integral approach. Here the finite amplitude effects are handled consistent with the one dimensional model by use of a taper function derived in Section 2.2.1 by differentiating the one dimensional solution.

The results are compared with experimental data of other investigators in Section 2.3. Then in Section 2.4, the experimental work performed in the present investigation is reported. Finally, the conclusions presented in Section 2.5 bring the discussion of the parametric receiving array to a close.

2.1 Weak Shock Theory Formulation of Parametric Receiving Array Axial Response

In the first quarterly progress report²⁹ of this investigation a derivation was given of a math model of parametric receiving array axial response. The signal was assumed to be a plane wave and the pump was assumed to be a one dimensional plane, cylindrical or spherical wave. Of primary interest are the plane and spherical wave formulations.

The derivation, as given, suffers from two problems. First, the secondary frequencies are shown to be produced by modulation of the pump by the signal and also by modulation of the signal by the pump but in the latter case the secondary frequencies produced appear to propagate with the signal. Actually, when the pump is spherical it modulates the signal along a spherical wave front and the interaction products should spread spherically, not as the plane wave signal. This fact, which is apparent from the scattering integral formulation, means that, even in this simple geometry, determination of the parametric receiving array axial response is not a one dimensional problem. The second problem is that in attempting to account for absorption by using modified weak shock theory, the absorption at the secondary frequencies cannot be correctly represented and must be introduced at the end of the derivation in ad hoc fashion.

The derivation as now presented is made rigorous by stipulating that the signal frequency be much smaller than the pump frequency, in which case the sum and difference frequencies are approximately equal to the pump frequency. The result of modulation of the signal by the pump may now be ignored. Two additional changes are introduced in the present derivation. The signal is assumed to spread with a large but finite radius of curvature and the signal is assumed to suffer no significant loss due to absorption within the region of interaction.

With the stated assumptions, the pump and signal wave field is given by

$$p = \rho_0 c_0^2 \epsilon \left\{ e^{-\alpha_0 (r-r_0)} \left(\frac{r_0}{r} \right)^n \sin \left[\omega_0 \left(t - \frac{r-r_0}{c_0} \right) - \Delta \phi \right] + \delta_0 \left(\frac{L+r_1}{L+r} \right) \sin \left[\omega_s t - \left(\frac{r-r_0}{c_0} \right) + \frac{\omega_s}{\omega_0} \Delta \phi \right] \right\} , \quad (1)$$

$$\text{where } \Delta \phi = \beta k_0 \int_{r_0}^r \frac{p(x)}{\rho_0 c_0^2} dx \quad (2)$$

represents the total retardation of the phase of a given wavelet resulting from the integrated effect of the disparity between the phase velocity and the small signal sound speed (group velocity).

Equation (1) may be rewritten with the substitutions

$$V = \frac{p}{\epsilon \rho_0 c_0^2} \left(\frac{r}{r_0} \right)^n e^{\alpha_0 (r-r_0)} , \quad (3)$$

$$y = \omega_0 \left(t - \frac{r-r_0}{c_0} \right) , \quad (4)$$

$$\phi = y + \Delta \phi , \text{ and} \quad (5)$$

$$\delta(r) = \delta_0 \left(\frac{r}{r_0} \right)^n \left(\frac{L+r_1}{L+r} \right) , \quad (6)$$

$$\text{as } V = \sin \phi + \delta(r) \sin \Omega \phi . \quad (7)$$

The formulation given above departs from the Earnshaw solution for the phase distortion of finite amplitude waves by the inclusion of the absorption term. However, when absorption is included in this manner the continuous portions of a wave containing shocks may be described as in weak shock theory (Blackstock, Ref. 18) with the result that the high and

low intensity results are matched in a single solution. Now,

$$\Delta \phi = \beta \epsilon k_0 \left\{ \int_{r_0}^r \left(\frac{r_0}{x} \right)^n e^{-\alpha_0(x-r_0)} dx \sin \phi + \delta_0 \int_{r_0}^r \frac{L+r_1}{L+x} dx \sin \Omega \phi \right\}; \quad (8)$$

so, letting

$$\sigma = \beta \epsilon k_0 \int_{r_0}^r \left(\frac{r_0}{x} \right)^n e^{-\alpha_0(x-r_0)} dx, \quad (9)$$

and

$$\sigma_s = \beta \epsilon k_0 \delta_0 \int_{r_0}^r \frac{L+r_1}{L+x} dx, \quad (10)$$

one obtains the expression for ϕ as

$$\phi = y + \sigma \sin \phi + \sigma_s \sin \Omega \phi. \quad (11)$$

(Based on reasoning given in Ref. 24, it may be that for long receiver ranges α_0 in Eq. 9 should be replaced by $2\alpha_0$. Normally, however, the difference is very small and for the present the form given is satisfactory.)

It is now observed from Eq. (11) that

$$|\phi - y| \leq \sigma + \sigma_s. \quad (12)$$

Now, if $\Omega(\sigma + \sigma_s) \leq 1$, the maximum phase error incurred by replacing ϕ by

y in the last term of Eq. (11) is 1 radian. Thus, the substitution can be made without appreciable effect on the solution and the interaction components may be obtained from Eq. (7) with ϕ given by

$$\phi = y + \sigma \sin \phi + \sigma_s \sin \Omega y . \quad (13)$$

With the substitution

$$y' = y + \sigma_s \sin \Omega y , \quad (14)$$

Eq. (13) becomes

$$\phi = y' + \sigma \sin \phi . \quad (15)$$

Then the first term of Eq. (7) assumes the form of the Earnshaw solution. Weak shock theory as formulated by Blackstock¹⁸ may now be applied. The solution expressed as a Fourier series is

$$\sin \phi = \sum_{n=1}^{\infty} B_n(\sigma) \sin n y' , \quad (16)$$

where the values for $B_n(\sigma)$ are those derived by Blackstock.¹⁸ Eqs. (15) and (16) may be substituted into Eq. (7) to give an explicit solution in terms of y' as

$$V = \sum_{n=1}^{\infty} B_n(\sigma) \sin n y' + \delta(r) \sin \Omega \left[y' + \sigma \sum_{n=1}^{\infty} B_n(\sigma) \sin n y' \right] . \quad (17)$$

It is now necessary only to extract the sum and difference frequency components which will be the coefficients of $\sin(1 \pm \Omega)y$. With the substitution of Eq. (14) into Eq. (17) and with the assumption that σ_s is small and further, that $\delta(r)\Omega\sigma_s$ is negligible, it is possible to write

$$V = \sum_{n=1}^{\infty} B_n(\sigma) \sin n (y + \sigma_s \sin \Omega y) + \delta(r) \sin \Omega \left[y + \sigma \sum_{n=1}^{\infty} B_n(\sigma) \sin n y \right] . \quad (18)$$

The only terms of the sums in Eq. (18) that significantly affect the sum and difference frequencies are the $n = 1$ terms. Thus, discarding the rest we have

$$V = B_1(\sigma) \sin(y + \sigma_s \sin \Omega y) + \delta(r) \sin \Omega (y + \sigma B_1(\sigma) \sin y) . \quad (19)$$

Equation (19) may be thought of as the sum of two broadband FM signals. The first term represents the modulation of the pump by the signal and the second represents the modulation of the signal by the pump.

Equation (19) may be written in exponential notation as

$$V = R_e \left\{ i B_1(\sigma) e^{-iy} e^{-i\sigma_s \sin \Omega y} + \delta(r) i e^{-i\Omega y} e^{-i\Omega \sigma B_1(\sigma) \sin y} \right\} . \quad (20)$$

Then, using the Fourier Bessel expansion we obtain

$$V = R_e \left\{ i B_1(\sigma) e^{-iy} \sum_{m=-\infty}^{\infty} J_m(\sigma_s) e^{-im\Omega y} + \delta(r) i e^{-i\Omega y} \sum_{k=-\infty}^{\infty} J_k[\Omega \sigma B_1(\sigma)] e^{-iky} \right\} . \quad (21)$$

Selecting only the $m = \pm 1$ and $k = \pm 1$ terms that give sum and difference frequencies and returning to real notation, we obtain

$$V = B_1(\sigma) J_1(\sigma_s) \left[\sin(1 + \Omega) y - \sin(1 - \Omega) y \right] + \delta(r) J_1[\Omega \sigma B_1(\sigma)] \left[\sin(1 + \Omega) y + \sin(1 - \Omega) y \right] . \quad (22)$$

It is now apparent that if $\Omega \ll 1$, the second term above may be neglected in comparison to the first. Thus, the result of modulation of the pump by the signal is retained and the result of the modulation of the signal by the pump, with its geometrical inconsistency, is discarded. The result for the sum and difference frequencies becomes

$$V_{\pm} = B_1(\sigma) J_1(\sigma_s) \sin(1 \pm \Omega) y \quad (23)$$

A similar result was obtained by Schaffer and Blackstock¹² for the case of an intense low frequency modulating a low amplitude high frequency. However, in the present case it has been possible to include the effects of shocks in the pump wave through the B_1 term derived from weak shock theory.

In dimensional notation the magnitudes of the sum and difference pressure signals become

$$|P_{\pm}| = \rho_0 c_0^2 \epsilon \left(\frac{r_0}{r} \right)^n B_1(\sigma) J_1(\sigma_s) e^{-\alpha_0(r-r_0)} \quad (24)$$

Normally, σ_s is small so that the small argument approximation of the Bessel function is valid and one may substitute

$$J_1(\sigma_s) \approx \frac{\sigma_s}{2} = \frac{\beta \epsilon k_0 \delta_0}{2} (L + r_1) \ln \left(\frac{L + r}{L + r_0} \right) \quad (25)$$

If the reference distance r_1 is taken to be the receiver location, then $r = r_1$. Furthermore, if L is large the value of σ_s reduces to the plane wave signal result

$$\begin{aligned} \sigma_s &\approx \beta \epsilon k_0 \delta_0 (r - r_0) \\ &\approx \beta \epsilon k_0 \delta_0 r \end{aligned} \quad (26)$$

The low amplitude limit of Eq. (24) is then

$$\begin{aligned}
 |P_{\pm}| &= \rho_o c_o^2 \epsilon \left(\frac{r_o}{r} \right)^n \frac{\beta \epsilon k_o \delta_o}{2} r e^{-\alpha_o (r-r_o)} \\
 &= \frac{\omega_o \beta p_1 p_2}{2 \rho_o c_o^3} \left(\frac{r_o}{r} \right)^n r e^{-\alpha_o (r-r_o)}, \quad (27)
 \end{aligned}$$

which agrees with the results of Berktaf and Shooter³⁰ and Berktaf and Al-Temimi⁸ for the cases $n = 1$ and $n = 0$, respectively, except that here ω_{\pm} and α_{\pm} have been approximated by ω_o and α_o .

2.1.1 Use of the Weak Shock Theory Results to Calculate Parametric Receiver Amplitude Response

The expressions derived in the previous section may be used to calculate the amplitude response of parametric receiver arrays that have interaction volumes either entirely in the pump nearfield or predominantly in the pump farfield. For intermediate cases where the receiver is in the farfield of the pump but there is a significant contribution from the nearfield, the plane wave and spherical wave solutions may be combined. However, it is necessary to correct the nearfield portion to account for spreading of the secondary signals. This is done by adding to the spherical wave solution the plane wave solution multiplied by the factor

$$F = \frac{1}{R} \left\{ \int_0^{R-R_o} \frac{R_o}{R-x} dx + \int_{R-R_o}^{R_o} dx \right\}, \quad (28)$$

where the quantities $(R - R_o)$ are replaced by R_o in the event that $R - R_o > R_o$. Similar factors were derived in Ref. 29 for the nearfield of the parametric transmitting array.

The two terms of the factor represent the portion of the nearfield beyond one Rayleigh distance from the receiver, the contributions from which undergo spherical spreading, and the portions within one Rayleigh distance which do not. The initial factor $1/R$ cancels the range dependence of the plane wave solution which is, in effect, replaced by the quantity in brackets.

The farfield contribution is calculated by using the spherical wave solution with a source radius of R_0 and an initial distortion based on the value of σ calculated at R_0 for the nearfield distortion.

2.2 Scattering Integral Evaluation of Parametric Receiving Array Axial Response

Because the determination of the secondary signal amplitude in a parametric receiving array with a piston pump transducer is not generally a problem involving only one spatial dimension, it is often desirable to use the scattering integral approach. In order to account for saturation effects it is then necessary to insert a taper function into the integral. Such a taper function is now derived.

2.2.1 Taper Function Derivation - It is tempting to use the pump fundamental harmonic coefficient $B_1(\sigma)$ as the taper function because this would make the source strength density proportional to the local pump amplitude. However, that approach would not include the diminishment of the secondary signal due to pump saturation as seen in the weak shock solution. Therefore, the alternative approach of deriving the taper function from the weak shock result is adopted.

The finite amplitude taper is calculated from the weak shock solution by taking the range derivative of the high intensity solution to obtain the one dimensional source strength density and then dividing by the low amplitude source strength density to normalize the result. Since only the high intensity taper is desired the spherical wave solution is range normalized before differentiating.

The two expressions (neglecting absorption) are, from the previous section with $\alpha_0 = \alpha_s = 0$, for the plane wave region of the pump,

$$P_{\pm} = \rho_0 c_0^2 \epsilon B_1(\sigma) J_1(\sigma_s) \quad , \quad (29)$$

and for the spherical wave region of the pump

$$\frac{r}{r_0} P_{\pm} = \rho_0 c_0^2 \epsilon B_1(\sigma) J_1(\sigma_s) \quad , \quad (30)$$

where

$$\sigma_s \approx \beta \epsilon k_0 \delta_0 \quad (31)$$

and σ is given by

$$\sigma = \beta \epsilon k_0 r \quad (32)$$

in the plane wave region, and by

$$\sigma = \beta \epsilon k_0 R_0 \left[1 + \ln(r/R_0) \right] \quad (33)$$

in the spherical wave region.

By differentiating the above expressions for P_{\pm} and $(r/r_0 P_{\pm})$ with respect to r , and normalizing the plane and spherical wave results by the respective low intensity limits, the two taper functions are obtained and are written,

$$T_p = \frac{d(\sigma B_1)}{d\sigma} \quad (34)$$

for a plane wave, and

$$T_s = B_1 + B_1'(\sigma) \sigma_0 \quad (35)$$

for a spherical wave.

The above taper functions are used in the numerical evaluation of the scattering integral as discussed in the next section. They differ from the simpler approach of using $B_1(\sigma)$ as the taper function in that they include the "absorption" of the secondary signal by the saturating pump.

It is noted however that the tapers were derived under the assumption that the pump and the secondary signals were propagating in a one dimensional fashion. In the case of a nearfield generated secondary

signal, which undergoes diffraction in passing to the farfield, it is not clear that the above tapers are valid. This question will be discussed further in the light of published experimental results in Section 2.3.

2.2.2 Numerical Evaluations of the Scattering Integral - The use of numerical volume integration in combination with the finite amplitude taper function is now described. The programming stems from a modification of the parametric transmitting array program utilized in this study which is, in turn, a modification of the Muir-Willette⁷ program. Because this investigation deals with describing axial response no attempt has been made to include off-axis response in the programs. However, the inclusion of the taper function in a program that handles off-axis geometries would be quite straightforward.

Actually, two different programs have been developed to evaluate the scattering integral. In the first, a volume integration over two coordinates is performed. In the second, closed form, high wave number approximations are used to reduce the solution to a single integration along the axis of the pump.

The geometry on which the programs are based is shown in Figure 1. It consists of a spherical wave signal source at an arbitrary distance (usually long) from the receiving hydrophone and a pump, assumed for convenience in programming to be a circular array with a plane wave nearfield and a spherical wave farfield. The nearfield of the pump projector is taken to be a collimated plane wave with an abrupt transition to spherical wave at the Rayleigh distance ($area/\lambda$) and an accompanying 90° phase shift.

The volume is formulated in cylindrical coordinates in the nearfield and in spherical coordinates in the farfield. The integral expression for the axial secondary pressure is

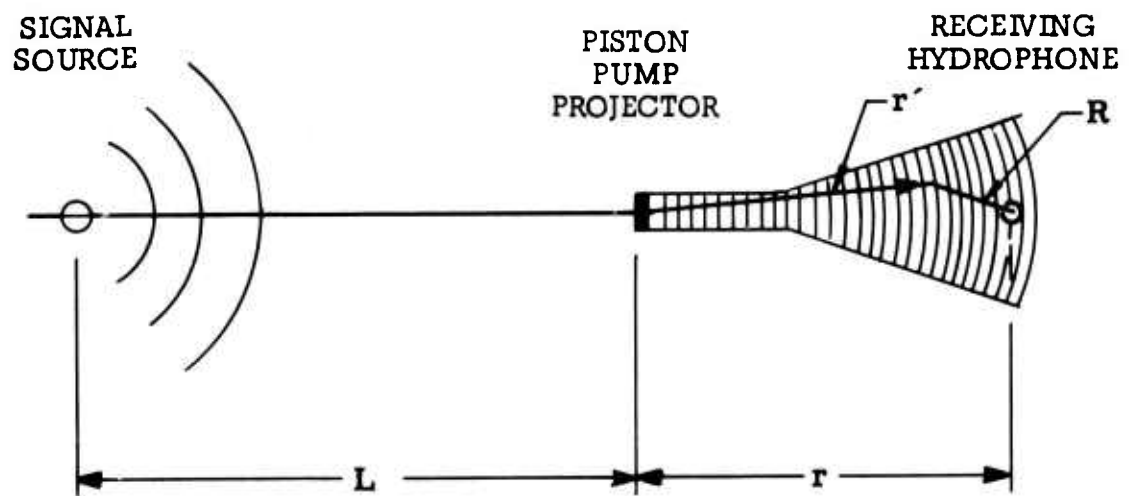


Figure 1. Parametric Receiving Array Geometry.

$$P_{\pm} = \frac{\beta \omega_{\pm} P_o P_s R_o}{2 \rho_o c_o^4} \left\{ T_p \int_{r_{\min}}^{R_o} \int_0^a \frac{r+L}{r'+L} \frac{e^{-\alpha_{\pm} R_1 + i k_o (R_1+r') \pm i k_s (R_1+R_{s1})}}{R_o R_1} x dx dr' \right. \quad (36)$$

$$\left. - T_s e^{i\pi/2} \int_{R_o}^r \int_0^{\theta_{\infty}} \frac{r+L}{r'+L} \frac{2 J_1(k_o a \sin \theta)}{k_o a} \frac{r'}{R} e^{-\alpha_{\pm} R + i k_o (R+r') \pm i k_s (R+R_s)} d\theta dr' \right\} ,$$

where T_p is the nearfield taper and T_s is the farfield taper given by Eqs. (34) and (35) respectively. The signal projector to field point ranges are

$$R_{s1} = \sqrt{(L+r')^2 + x^2} , \quad (37)$$

and

$$R_s = \sqrt{L^2 + r'^2 + 2L r' \cos \theta} , \quad (38)$$

while

$$R_1 = \sqrt{x^2 + (r-r')^2} , \quad (39)$$

is the source to field point range in the nearfield, and

$$R = \sqrt{r^2 + r'^2 - 2r r' \cos \theta} \quad (40)$$

is the source to field point range in the farfield. The lower limit in the range integration is r_{\min} , the shadow length of the pump transducer given by $r_{\min} = \text{area}/\lambda_s$.

The basic parametric receiver program utilizes a two dimensional integration of the above equation. Unfortunately, the phase variations of the integrand are so rapid at high pump frequencies that it is extremely difficult and expensive to obtain convergence of the integral.

To overcome this difficulty a high wave number approximation of the θ integration and an approximate closed form x integration have been incorporated into a second version of the program. This single integral program has been found to give equivalent results to those of the double integration but with considerably improved convergence.

The angle integration is approximated as follows: let

$$I_{\theta} = \int_0^{\theta_{\infty}} \frac{2 J_1(k_0 a \sin \theta)}{k_0 a \sin \theta} \frac{e^{-\alpha_{\pm} R \pm i k_s R_s}}{R} \sin \theta d\theta \quad (41)$$

Provided that

$$k_s \left[\sqrt{L^2 + r^2 + 2Lr \cos \theta_{\infty}} - (L+r) \right] < 1, \quad (42)$$

it is permissible without loss of accuracy, to let

$$R_s \cong L + r^2 \quad (43)$$

Then, with the substitution

$$\frac{\sin \theta d\theta}{R} = \frac{dR}{r r'} \quad (44)$$

the integral may be written

$$I_{\theta} = e^{\pm i k_s (L+r^2)} \int_{R(0)}^{R(\theta_{\infty})} \frac{2 J_1(k_0 a \sin \theta)}{k_0 a \sin \theta} e^{-\alpha_{\pm} R \pm i k_{\pm} R} \frac{dR}{r r'} \quad (45)$$

where θ is regarded as a function of R .

Integration by parts now gives

$$I_{\theta} = \frac{e}{r r'} \left\{ \frac{2 J_1(k_0 a \sin \theta)}{k_0 a \sin \theta} e^{-\alpha_{\pm} R} \frac{e^{i k_{\pm} R}}{i k_{\pm}} \right\}_{R(0)}^{R(\theta_{\infty})} - \frac{1}{i k_{\pm}} \int_{R(0)}^{R(\theta_{\infty})} \frac{d}{dR} \left[\frac{2 J_1(k_0 a \sin \theta)}{k_0 a \sin \theta} e^{-\alpha_{\pm} R} \right] e^{i k_{\pm} R} dR \quad (46)$$

The second term could be repeatedly integrated by parts but would only produce terms of higher order in k_{\pm}^{-1} . Consequently, it is neglected and since the first term is zero at the upper limit, the integral reduces to

$$I_{\theta} \approx - \frac{e}{r r'} e^{\pm i k_s (L+r')} e^{-\alpha_{\pm} (r-r')} \frac{e^{i k_{\pm} (r-r')}}{i k_{\pm}} \quad (47)$$

The above approximation is valid for

$$k_{\pm} r' > k_{\pm} \left(\frac{k_0}{k_{\pm}} R_0 \right) \quad (48)$$

The x integration in the nearfield is represented by

$$I_x = \int_0^a e^{-\alpha_{\pm} R_1 + i k_{\pm} R_1 \pm i k_s R_{s1}} \frac{x dx}{R_1} \quad (49)$$

With the approximation

$$R_{s1} \approx L + r' \quad (50)$$

the integral may be evaluated analytically.

The variable of integration is transformed to R_1 by the relation

$$\frac{x dx}{R_1} = dR_1 \quad (51)$$

Then,

$$\begin{aligned}
 I_x &= e^{ik_s(L+r')} \int_{R_1(0)}^{R_1(a)} e^{-\alpha_{\pm} R_1 + ik_{\pm} R_1} dR_1 \\
 &= \frac{e^{ik_s(L+r')}}{ik_{\pm} - \alpha_{\pm}} \left[e^{(-\alpha_{\pm} + ik_{\pm}) \sqrt{a^2 + (r-r')^2}} - e^{(-\alpha_{\pm} + ik_{\pm})(r-r')} \right]. \quad (52)
 \end{aligned}$$

With α_{\pm} treated as small compared to k_{\pm} , the result becomes

$$I_x = \frac{e^{ik_s(L+r')}}{ik_{\pm}} e^{-\alpha_{\pm}(r-r')} \left[e^{ik_{\pm} \sqrt{a^2 + (r-r')^2}} - e^{ik_{\pm}(r-r')} \right]. \quad (53)$$

The above expressions used to reduce the integration to a single range integration, have produced excellent results. Because of the convergence problems already noted, the single integration program is believed to be inherently more accurate than the double integration version, at least for pump frequencies much higher than the signal frequency.

The scattering integral and one dimensional models give nearly the same results, demonstrating that the handling of the finite amplitude taper is consistent. The scattering integral approach is, of course, more accurate in handling geometry. With the reduction to a single integration the scattering integral computer program is very fast and inexpensive to use. Results obtained using the single integration program are compared with available experimental results in the following section.

2.3 Comparison of Theoretical Results with Experimental Data of Other Investigators

Only two sources of experimental data showing the effects of pump saturation on parametric receiver axial response have been identified. One source is an article published by Berktaf and Al-Temimi⁸ which contains

secondary amplitude response curves for a pump frequency of 2850 kHz and several different signal frequencies. In this experiment, the receiving hydrophone was placed at the approximate nearfield collimation distance of the pump transducer. The other source is experimental data obtained by Konrad, Mellen and Moffett.⁹

Earlier efforts by the present author to compare theory with the data reported by Konrad, Mellen and Moffett led to confusion because even the low amplitude data did not agree with any available theory. After the discrepancies were brought to the attention of the authors, Moffett concluded that a better estimate of the hydrophone sensitivity could be made. He did so and was kind enough to provide revised data³², not only for the originally reported experiment which used a 620 kHz pump and a 44 kHz signal, but also for experiments performed at the same time using two additional signal frequencies, 30 and 13.5 kHz. It is the revised data that are discussed here.

Theoretical calculations were made using the scattering integral approach detailed in Section 2.2.2. Finite amplitude effects were accounted for by use of the taper function defined in Section 2.2.1. The data so obtained are represented by the solid curves in Figures 2 through 5.

Figure 2 shows the comparison with a typical data set from Berkta and Al-Temimi. Figures 3 through 5 show comparisons with data of Konrad, Mellen and Moffett for two different ranges, 5.3 m and 9.1 m, and three different signal frequencies. The data for the 44 kHz signal frequency replace the ones originally reported.

Figure 2 shows a definite disagreement between theory and experiment for the data of Berkta and Al-Temimi, although the theory does fit the low amplitude data. Barring experimental error these data indicate that the present taper function results in too much loss due to saturation for the interaction in the nearfield of the pump. The data actually agree closely with the theory given by Bartram which gives similar results to what is obtained by the present methods if the taper function is taken to be equal to the fundamental component amplitude of the pump signal, rather than using the taper function derived in Section 2.2.

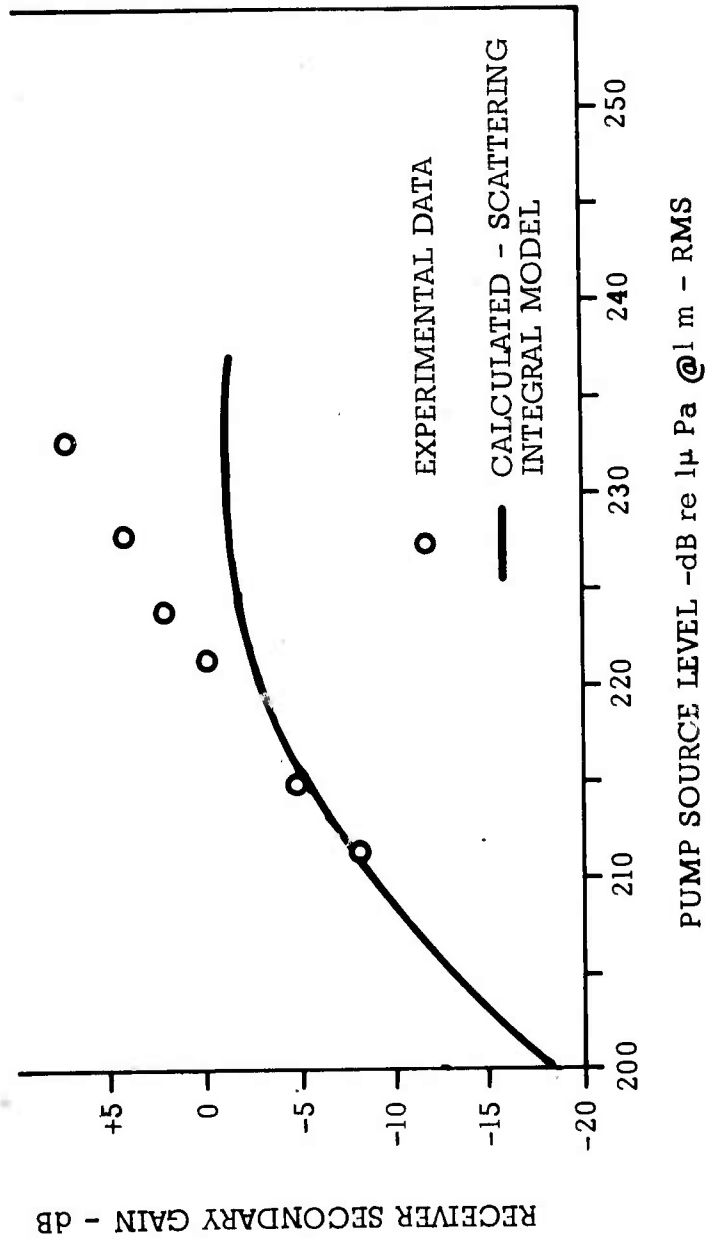


Figure 2. Comparison of Theory and Experimental Data of Berkay and Al-Temimi (Ref. 8). Pump Frequency = 2850 kHz, Signal Frequency = 33 kHz, Pump to Hydrophone Range = 1.8m, $R_0 = 1.7m$, Source to Hydrophone Range = 10m.

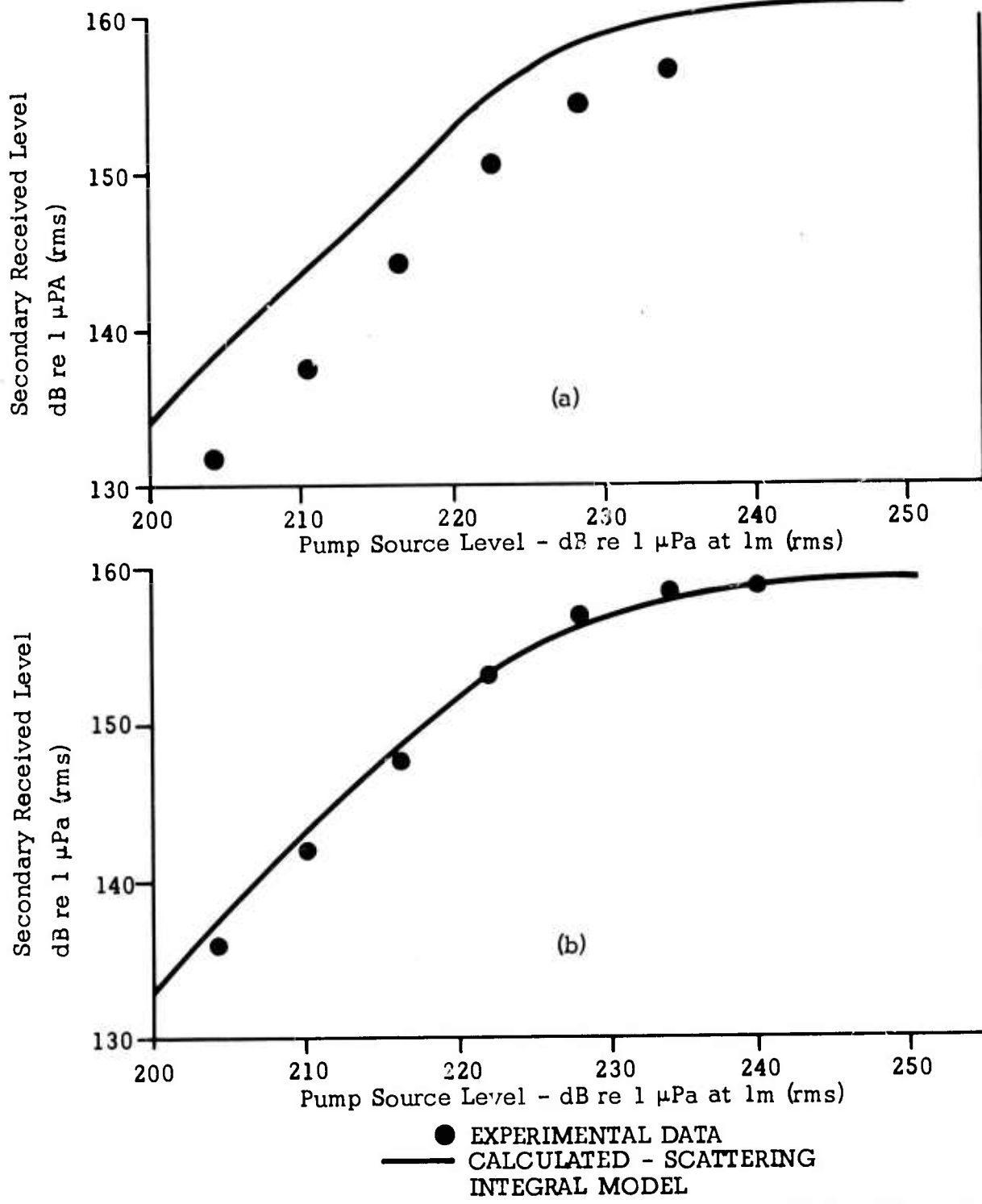


Figure 3. Comparison of Theory and Experimental Data of Konrad, Mellen and Moffett (Refs 9 and 32). Pump Frequency = 620 kHz, Signal Frequency = 44 kHz, Source to Hydrophone Range = 21.5m, $R_0 = 3.25m$, Signal Level at Hydrophone = 162.2 dB re 1 μ Pa

- (a) Pump to Hydrophone Range = 5.3m
- (b) Pump to Hydrophone Range = 9.1m

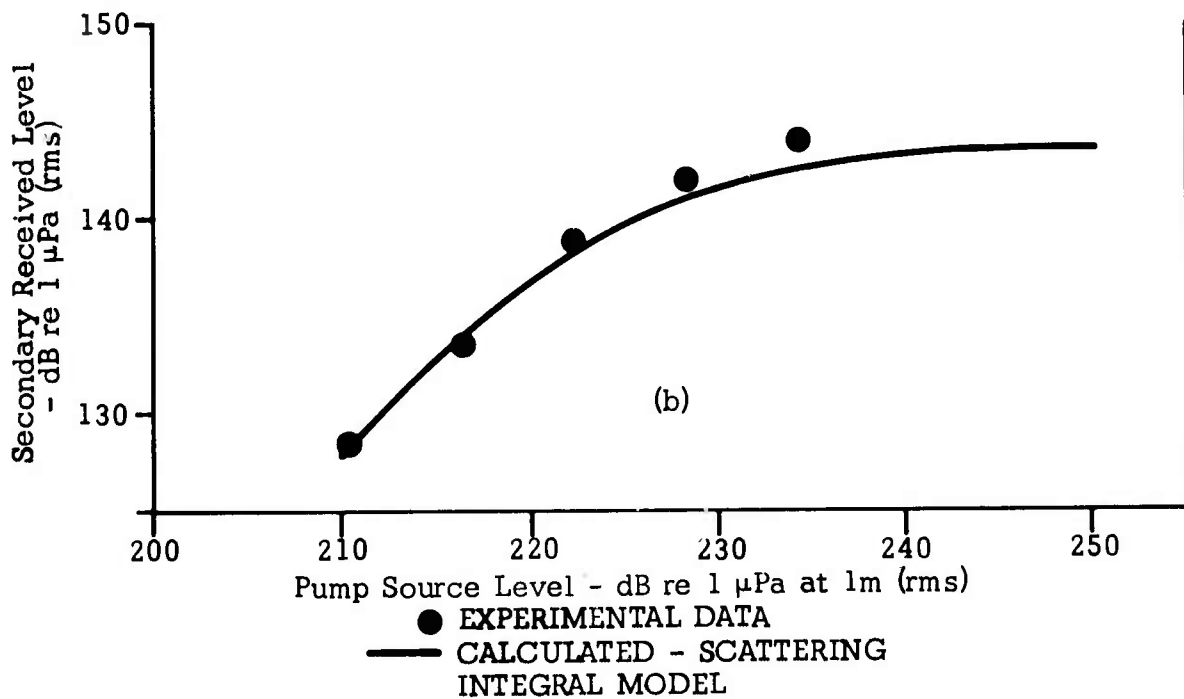
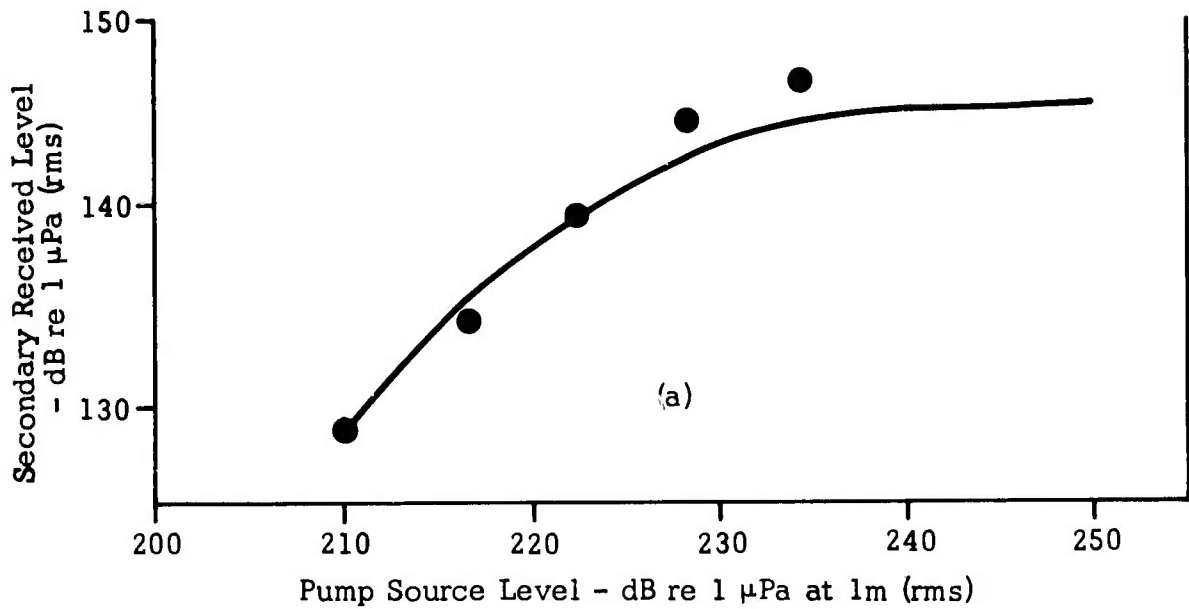
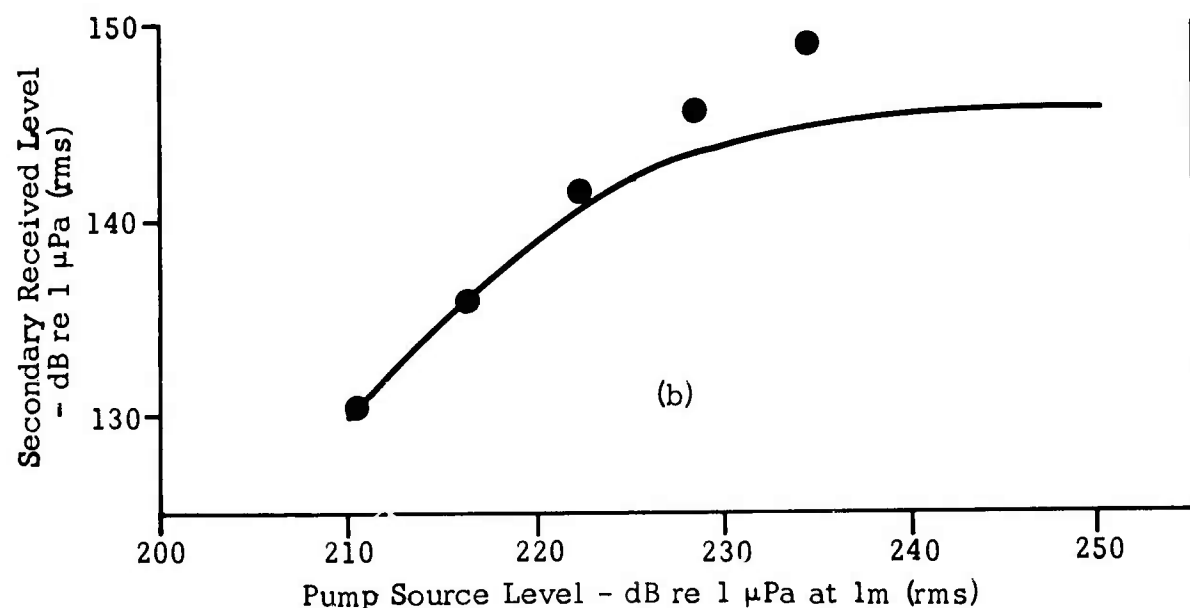
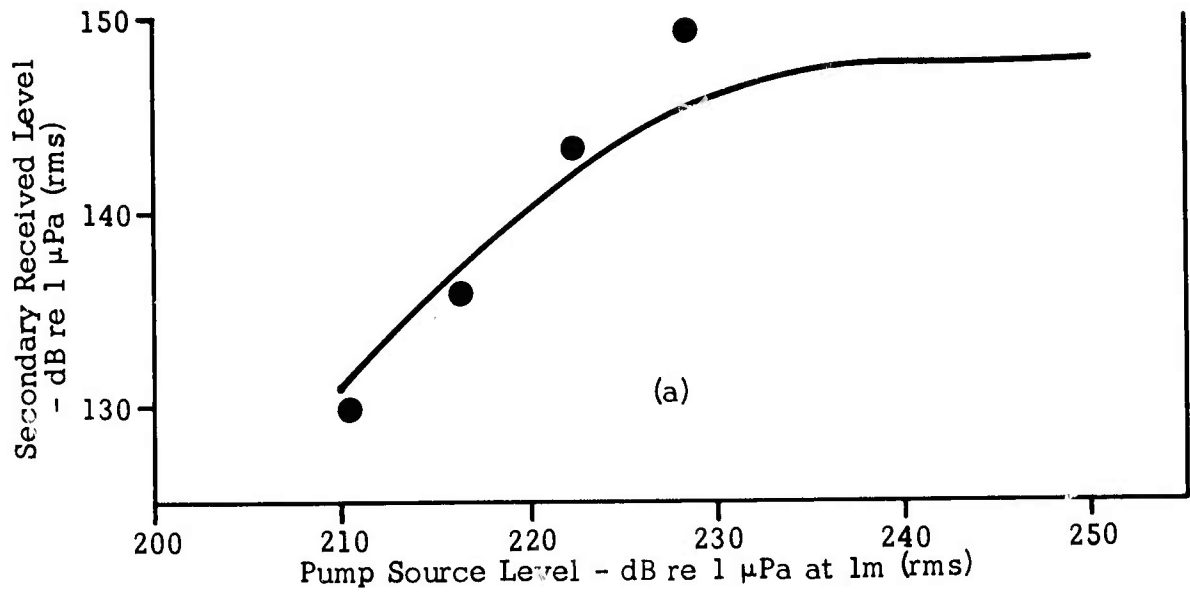


Figure 4. Comparison of Theory and Experimental Data of Konrad, Mellen and Moffett (Ref 32). Pump Frequency = 620 kHz, Signal Frequency = 30 kHz, Source to Hydrophone Range = 21.5m, $R_0 = 3.25$ m, Signal Level at Hydrophone = 147.2 dB re 1 μ Pa

(a) Pump to Hydrophone Range = 5.3m

(b) Pump to Hydrophone Range = 9.1m



● EXPERIMENTAL DATA
 — CALCULATED - SCATTERING INTEGRAL MODEL

Figure 5. Comparison of Theory and Experimental Data of Konrad, Mellen and Moffett (Ref 32). Pump Frequency = 620 kHz, Signal Frequency = 13.5 kHz, Source to Hydrophone Range = 21.5m, $R_0 = 3.25m$, Signal Level at Hydrophone = 149.8 dB re 1 μPa

- (a) Pump to Hydrophone Range = 5.3m
- (b) Pump to Hydrophone Range = 9.1m

In contrast to the Berkday, Al-Temimi results the Konrad, Mellen and Moffett data support the present theory quite well. Figure 3, which gives the 44 kHz signal frequency data, shows excellent agreement at the 9.1 m hydrophone range and good agreement so far as curve shape is concerned, but a 7 dB offset at the 5.3 m hydrophone range. Because the offset does not appear in any of the five other data sets it is undoubtedly the result of some bias error in the experiment. Figure 4 shows quite good agreement between theory and experiment for the 30 kHz signal frequency experiment.

It is interesting to note that for either range, if the 44 kHz data are overlaid on the 30 kHz data and allowed to move vertically, the two sets may be made to line up almost perfectly. That is, the experimental saturation curves have the same shape. This shape represents slightly less saturation than the theory, particularly at the 5.3 m range, but the agreement is considered quite good. Here, particularly at the 9.1 m range, the present theory gives a much better fit than one that uses the fundamental component amplitude as the taper.

Figure 5 gives the data for a signal frequency of 13.5 kHz. These data show a shape considerably different from that of the other sets. Since only the signal frequency was changed, and there is no known reason for this to appreciably affect the shape of the saturation curve, it is believed that the difference may have been caused by the electronics. Therefore, considerably more weight is placed on the excellent fits obtained in the 44 kHz and 30 kHz data.

It is concluded that the data of Konrad, Mellen and Moffett generally support the theory presented in Section 2.2 but that the Berkday and Al-Temimi data do not. The derivation of the theory is based on the assumption of farfield propagation and the possibility exists that the near-field may, in general, exhibit a different type of behavior. This may account for the different behavior evidenced in the Berkday, Al-Temimi data. This possibility will be discussed further in Section 2.5.

2.4 Experimental Measurement of Parametric Receiver Amplitude Response

Insofar as directivity measurements are not required in the study of amplitude response, it is possible to set up a well aligned and controlled experiment in a tank. Such an experimental arrangement was effected in the AMETEK test pool and is shown schematically in Figure 6. A 3.8 x 11.4 cm pump transducer was used, operating at a frequency of 700 kHz. Typical beam patterns for this projector are shown in Figures 7 and 8. A 50 kHz signal source was positioned at one end of the pool 7.9 m behind the 700 kHz pump. The narrow beam pump projector was driven by a 200 watt power amplifier from Scientific System Technology, Inc. The pump signal and intermodulation products at 650 and 750 kHz were received by an E-8 hydrophone at a distance of 3.7 m from the pump. The 50 kHz signal was quite intense by comparison with the usual situation in parametric receivers. Consequently, it was quite easy to separate the sidebands from the pump by narrow band filtering. The pump was operated in a pulsed mode, a compromise necessitated by the transducer design. However, the precaution of using a long enough pulse to ensure the gate sidebands being well below the secondary signals was taken. A 4 ms pulse proved to be adequate and was used.

The narrow band filtering was accomplished by passing the composite signal into a Hewlett-Packard Model 310A wave analyzer set on a bandwidth of 200 Hz. The output signal was passed to standard calibration equipment and measured on a logarithmic plotter. The pump and the sum and difference frequencies were measured by peaking the wave analyzer response on each frequency in turn. The measurements were made absolute by passing a 4 ms pulse of known amplitude at 700 kHz through the signal path.

Only one set of data were obtained before the transducer failed due to being overdriven and efforts to build a second unit were unsuccessful. The experimental data are shown in Figures 9 and 10. Figure 9 shows the pump fundamental component amplitude response. The solid curve is theory (Ref. 24). These data are quite consistent and show a definite nonlinearity

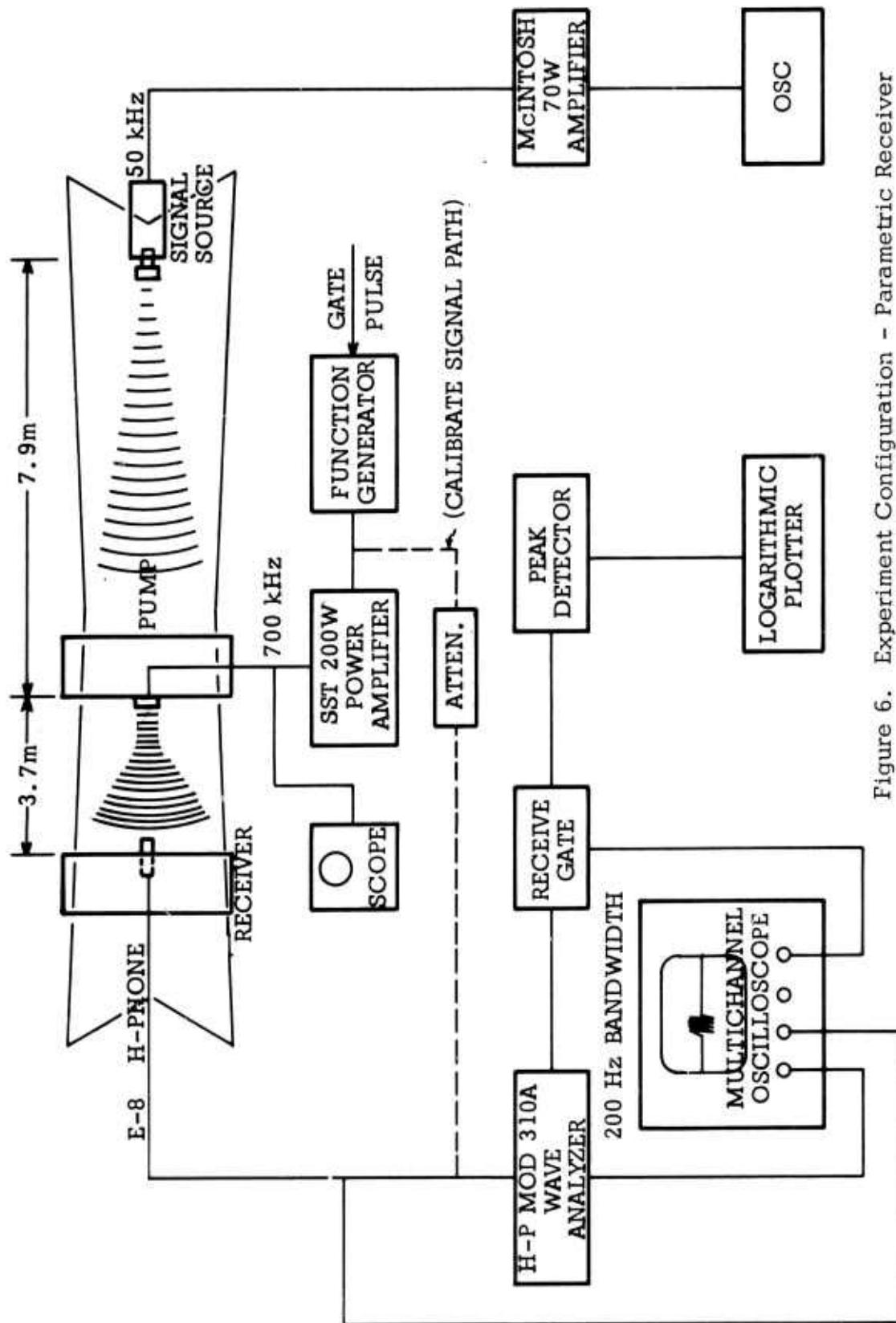


Figure 6. Experiment Configuration - Parametric Receiver Amplitude Response

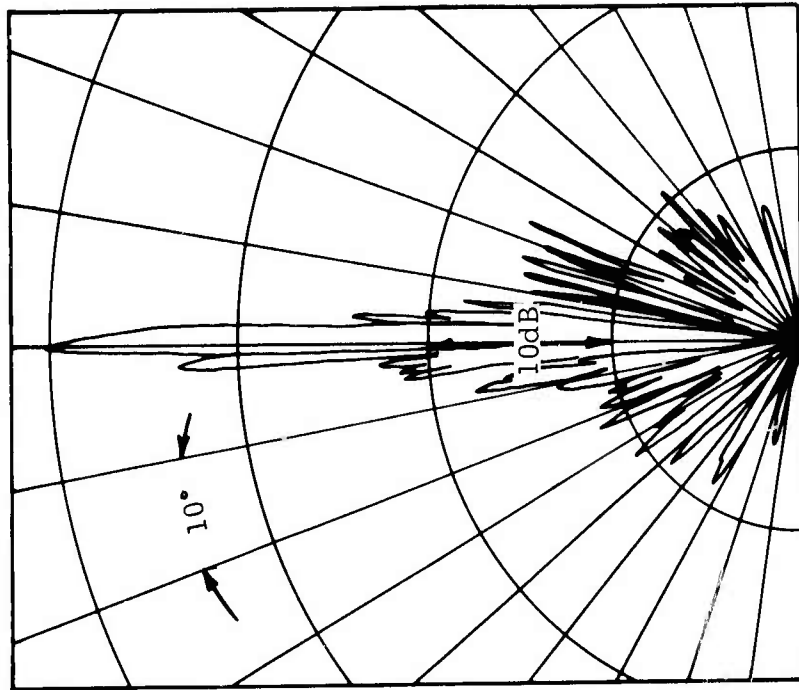


Figure 8. Pump Horizontal Farfield Directivity Pattern at a Frequency of 700 kHz.

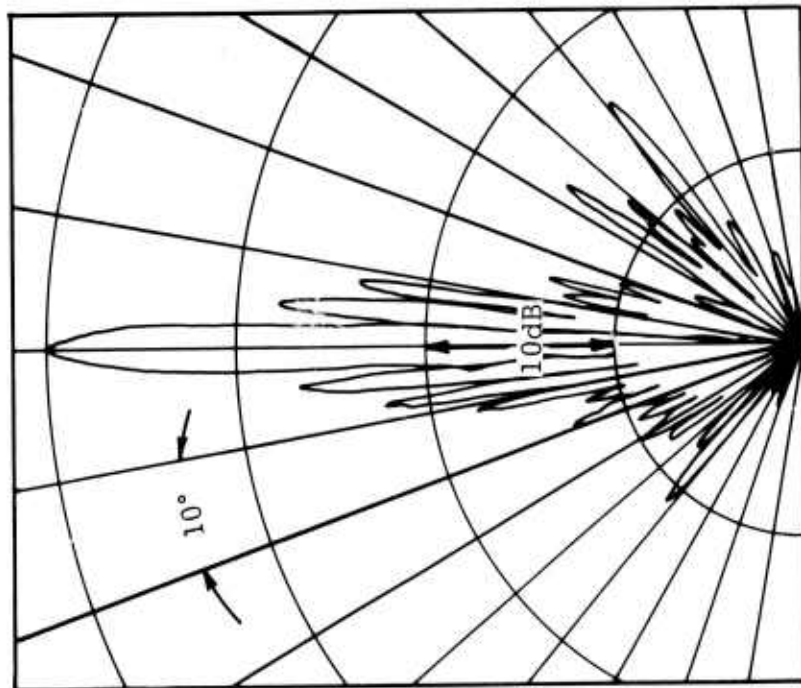


Figure 7. Pump Vertical Farfield Directivity Pattern at a Frequency of 700 kHz.

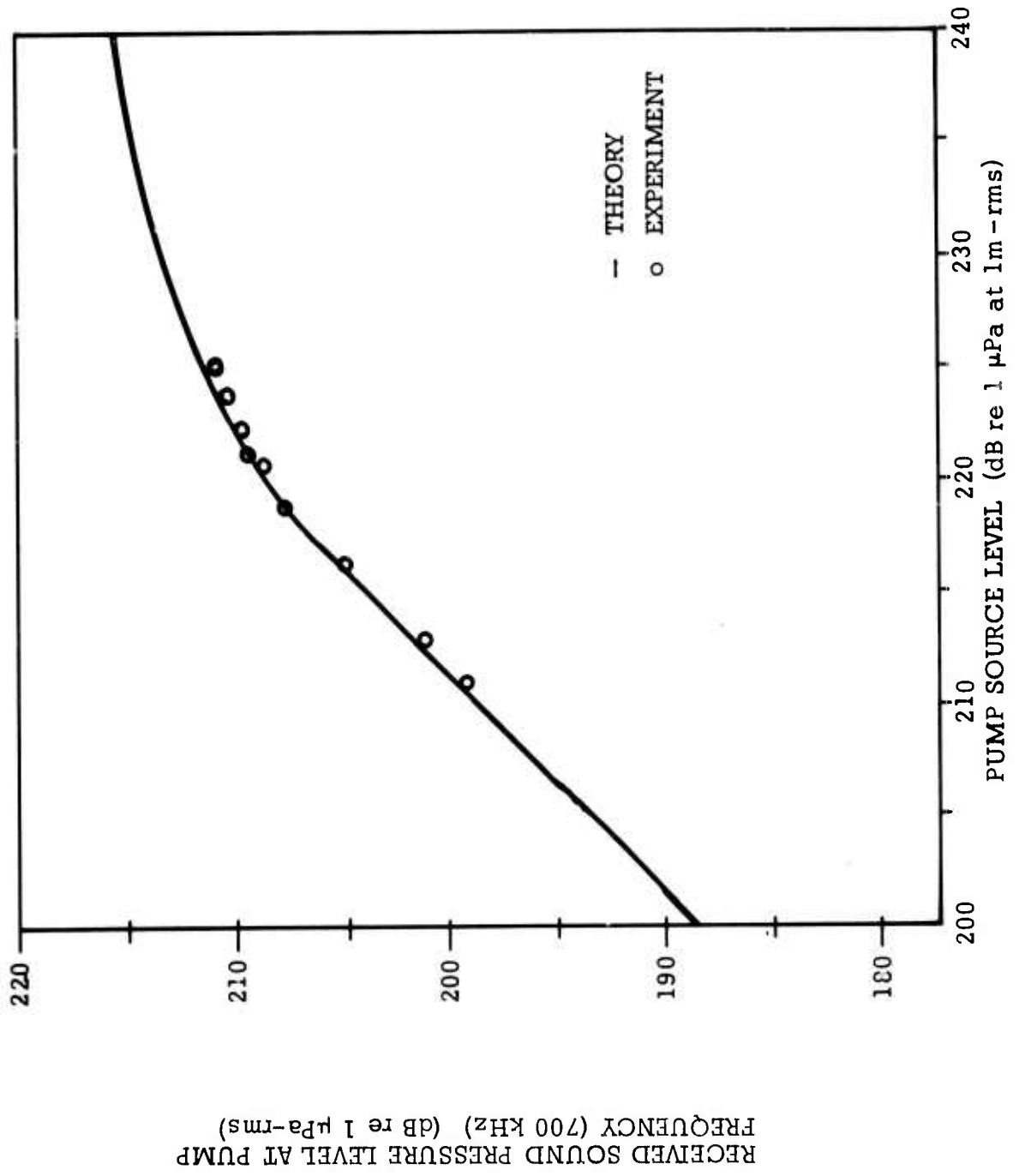


Figure 9. Pump Amplitude Response

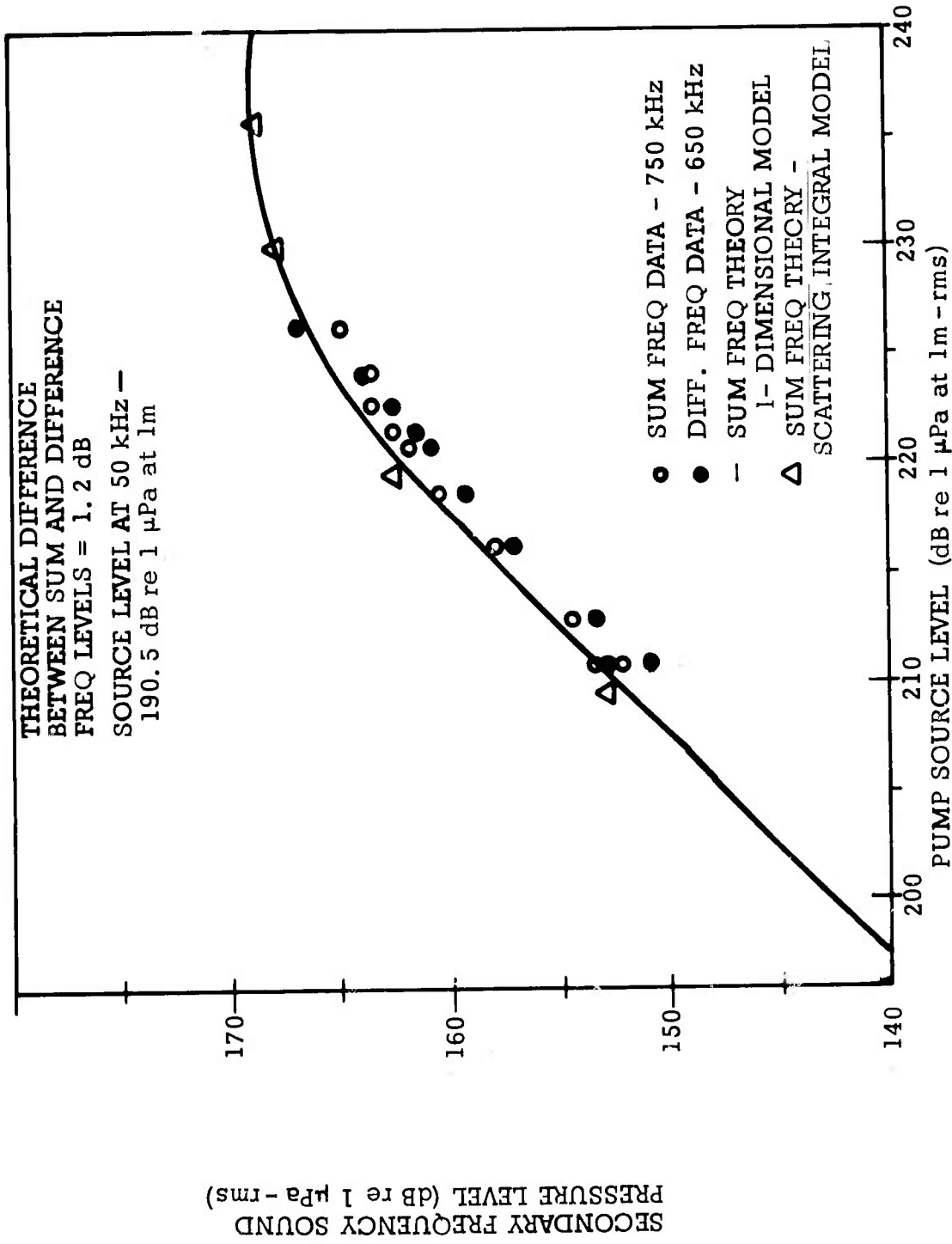


Figure 10. Secondary Frequency Amplitude Response.

at high source level in agreement with theory. Figure 10 shows the secondary frequency amplitude data. Although these data are not as consistent as those for the pump, agreement with the theory is indicated. The solid curve is based on the one dimensional theory (Section 2. 1). Also shown on the plot are points calculated by the scattering integral method.

In the experimental measurements the source level of the 50 kHz signal was 190.5 dB re $1\mu\text{Pa}$ at 1 m. This was determined by pulsing the source and measuring the amplitude prior to the onset of reflections. In the actual parametric receiver experiment the signal was continuous and considerable standing waves were present. In spite of this the data agree with theory based on the free-field source level. The receiving array is insensitive to reflections not collinear with the pump.

2.5 Conclusions: Parametric Receiving Array Finite Amplitude Taper

Two models for predicting parametric receiving array axial response have been derived. One is based on a one dimensional weak shock theory model with a simple correction for nearfield geometry. The other is based on the scattering integral approach.

Both models have weak shock theory as the basis for predicting saturation effects. The main result of the weak shock theory analysis is that the pump signal is distorted by finite amplitude effects. At the same time each distortion component of the pump signal is frequency modulated by the signal frequency. As the pump fundamental component, which is the only one resulting in sum and difference frequencies, attenuates, the sidebands are also attenuated. Thus, in the scattering integral approach, the taper function is not a positive definite quantity but may become negative, representing a diminuation of sideband energy due to pump saturation.

This view of parametric receiving array taper seems physically reasonable, at least for one dimensional propagating waves. It is supported experimentally by the results of Konrad, Mellen and Moffett and by the experimental results obtained during the present investigation, although the pump amplitudes obtained in the latter work were not high enough to make the results really definitive.

The present taper theory applied to the pump nearfield gives results that sharply disagree with data presented by Berkay and Al-Temimi. Because application of the theory to the nearfield is not so readily justifiable as its application to the farfield, this disagreement is taken as an indication that the theory should only be applied to cases in which the receiving hydrophone is well in the pump's farfield. The data that do support the theory are from experiments in which the receiving hydrophone was well in the farfield of the pump.

The data of Berkay and Al-Temimi tend to support the hypothesis that the taper in the nearfield should be the amplitude of the pump fundamental component as a function of range. It is tempting to speculate that this may, in fact, be the nearfield taper and that this should be combined with the present farfield theory to give a more comprehensive model. The present author has refrained from doing this because the justification would be purely empirical and there is only one available supporting experiment. Should any additional nearfield data become available the question of what taper applies to the nearfield should again be addressed. In the meantime the present model is believed to adequately describe the axial response of parametric receivers in which the receiving hydrophone is well in the farfield of the pump.

The scattering integral approach has been the principal method of predicting parametric transmitting array performance, whether by numerical volume integration or by approximating the integral by some simpler form. In this approach the concept of a taper function is useful because it enables the finite amplitude effects to be described in terms of a range and amplitude dependent diminution of the source strength density.

Taper functions have previously been applied successfully only to simplified integration models - for example, the Mellen and Moffett¹³ model. It was the objective of the present work to apply the taper concept to the full volume integration approach. It would then be seen whether, by more detailed account of geometry and inclusion of the directivity factor in calculating the taper function, the results would differ significantly among various taper functions and whether they would differ from the results obtained by Mellen and Moffett.

Several taper functions have been compared, including a new one derived using weak shock theory. It should be noted, however, that none of the taper functions considered includes account of possible higher order interactions that may cause the secondary frequency to be depleted at extremely high amplitudes. Such effects are included in a one dimensional model proposed by Fenlon.¹⁷ That model is compared with the results of Mellen and Moffett in Ref. 13 wherein it is shown that significant differences are expected at extremely high amplitudes. In order to include these higher order interactions in the scattering integral approach it would be desirable to derive a taper function from the Fenlon results in a manner similar to the treatment of the parametric receiving array in the previous sections. However, that is beyond the scope of the present work.

In Section 3.1 the derivation is given for a taper function based on a time domain theory for difference frequency generation given by Merklinger.¹⁴ Because the taper is based on the primary intensity it will be referred to as the

"Intensity Taper Function." As mentioned in Section 1.0, the phase reversed parametric array data of Mellenbruch and Muir¹ are useful for trying out a taper function concept. Therefore, the phase reversed version of the taper function is also derived.

Numerical results are compared with the phase reversed data in Section 3.2. In Section 3.3 several of the proposed taper functions are compared. Results of parametric array calculations are compared in Section 3.4.

3.1 Derivation of the Intensity Taper Function

Merklinger¹⁴ has shown that the source function for secondary radiation in the lower sideband is proportional to the time derivative of the total intensity under the modulation envelope. The difference frequency source function is obtained by extracting the Fourier coefficient at the difference frequency

$$q_d \propto \int_0^{\pi} \frac{dI}{dy} \cos y \, dy \quad , \quad (54)$$

where

$$y = \omega_d \left(t - \frac{x}{c} \right) \quad . \quad (55)$$

The intensity variation in the envelope is assumed to be unaffected by the presence of the lower sideband. Therefore, if the primary spectrum consists of two frequencies of equal amplitude, $I(y)$ may be calculated from theory for an initially monochromatic wave at the carrier frequency of intensity amplitude $I_0(y)$. This is done using a modified form of weak shock theory described by Lockwood²⁴ in which the ordinary weak shock theory¹⁸ solution for $B_1(\sigma)$ is used, with σ for directive spherical waves replaced by

$$\sigma = \beta \epsilon D(\theta) k r_0 \int_{r_0}^r \frac{e^{-2\alpha(x-r_0)}}{x} \, dx \quad , \quad (56)$$

and the fundamental component amplitude $B_1(\sigma)$ multiplied by $e^{-\alpha_0(r-r_0)}$. The problem of obtaining $I(y)$ for the ordinary and the phase reversed parametric arrays is now reduced to finding appropriate weak shock theory expressions for the intensity variation as a function of σ .

The intensity in an initially sinusoidal wave without reflection is obtained by assuming that continuous parts of the wave are described by

$$\begin{aligned}
 V &= \sin \phi, \text{ where} \\
 \phi &= \omega_c(t-x/c) + \sigma \sin \phi = y + \sigma \sin \phi.
 \end{aligned}
 \tag{57}$$

The dependence of the total intensity is then

$$\begin{aligned}
 I &\propto \int_0^\pi \sin^2 \phi \, dy \\
 &= 2 \int_{\phi_{\min}}^\pi (\sigma \sin \phi) \sin \phi \cos \phi \, d\phi \\
 &= -\frac{2}{3} \sigma \sin^3 \phi_{\min} + \frac{\pi}{2} + \phi_{\min} \sin^2 \phi_{\min} + \frac{1}{2} \sin \phi_{\min} \cos \phi_{\min} - \frac{\phi_{\min}}{2},
 \end{aligned}
 \tag{58}$$

where ϕ_{\min} is a solution of

$$\phi_{\min} = \sigma \sin \phi_{\min}.
 \tag{59}$$

It is convenient to normalize the preceding expression to a zero distortion value of unity. Then we have

$$\frac{I}{I_0} = 1 + \frac{2}{3\pi} \sigma \sin^3 \phi_{\min} + \frac{1}{\pi} \sin \phi_{\min} \cos \phi_{\min} - \frac{\sigma}{\pi} \sin \phi_{\min}.
 \tag{60}$$

An expression for the intensity in an initially sinusoidal wave with reflection at a range corresponding to $\sigma = \sigma_r$ is now derived. It is assumed that after inversion straight lines remain straight. Otherwise, continuous parts are described by

$$V = \sin \phi, \text{ where}$$

$$\phi = y + \sigma_E \sin \phi, \text{ and} \tag{61}$$

$$\sigma_E = \sigma - 2\sigma_r.$$

We redefine ϕ_{\min} as the shock phase corresponding to the shock that forms subsequent to reflection; ϕ_{\max} is the phase corresponding to the pre-reflection shock, $\phi_{\max} = \pi - \phi_{\min}$. (Note that the time origin has been shifted by π to put the new shock in the usual place.)

We now have the intensity given by

$$\begin{aligned} I &\propto \int_{y(\phi_{\min})}^{y(\phi_{\max})} \sin^2 \phi \, dy + \int_{y(\phi_{\max})}^{\pi} \left[\sin \phi_{\min} \left(\frac{\pi - y}{\pi - y(\phi_{\max})} \right) \right]^2 dy \\ &= \frac{\phi_{\max}}{2} - \frac{1}{4} \sin^2 \phi_{\max} - \frac{\phi_{\min}}{2} + \frac{1}{4} \sin^2 \phi_{\min} \frac{-\sigma_E}{3} \\ &\quad \left(\sin^3 \phi_{\max} - \sin^3 \phi_{\min} \right). \end{aligned} \tag{62}$$

The normalized expression in terms of ϕ_{\max} and ϕ_{\min} is

$$\frac{I}{I_0} = \frac{\theta_{\max} - \theta_{\min}}{\pi} - \frac{1}{2\pi} \left(\sin^2 \theta_{\max} - \sin^2 \theta_{\min} \right) \quad (63)$$

$$+ \frac{2}{3\pi} \theta_{\min} \sin^2 \theta_{\min} + \frac{2}{3\pi} (\pi - \theta_{\max}) \sin^2 \theta_{\max} .$$

In case $\theta_{\max} \leq \theta_{\min}$, the preceding expression breaks down. The straight segment corresponding to the pre-reflection shock overtakes the zero and a sawtooth is formed instantly. The normalized intensity turns out to be

$$\frac{I}{I_0} = \frac{2 \sin^2 \theta_{\max}}{3} \frac{\pi^2}{\left(\pi - \theta_{\max} + \sigma_E \sin \theta_{\max} \right)^2} . \quad (64)$$

The present taper function (Eq. 60) is compared with other proposed taper functions in Section 3.3. First, however, results computed using the taper function (Eqs. 63 and 64) are compared with experimental data for the phase reversed parametric array.

3.2 Numerical Results - Phase Reversed Parametric Array

The numerical integration program of Muir and Willett⁷ has been cast into a form that accepts a finite amplitude taper function. The taper function which is, of course, amplitude dependent, is calculated as a function of the angular coordinate so that the directivity pattern of the primary radiation weights the amplitude. Thus, the axial taper is much more extreme than the taper at, for example, the -3 dB points.

Several methods of accounting for nearfield saturation effects have been tried. The best results have been obtained by treating the nearfield as a collimated plane wave out to the Rayleigh distance. The expression for σ is given in Eq. (70) of Section 3.3. It is interesting to note that if spherical wave theories are used the same nearfield distortion (assuming $\alpha R_0 \ll 1$) may be obtained by letting $r_0 = R_0/e$.

As a preliminary calculation to check out the program and the taper function derived in Section 3.1, theoretical curves were calculated to compare with the phase reversed parametric array data of Mellenbruch and Muir¹. The results are shown in Figure 11. The data are for a 14 kHz difference frequency produced by a source operating at 424 and 438 kHz and reflected at a range of 4 yards. Results using a less sophisticated theory were previously reported by Lockwood.²⁸ The present results agree considerably better with experiment than the previous ones did. However, the agreement at the highest amplitudes is not as good as had been hoped for. Anomalous nearfield effects are suspected as the reason.

3.3 Comparison of Various Taper Functions

Fenlon¹⁷ has given a list in consistent notation of several taper functions that have been proposed by various authors for use in conjunction with quasi one dimensional geometrical models. Those from Fenlon's list that apply to the farfield of the parametric source are now compared.

First, it is noted that all of the functions in the list may be expressed in the form

$$T = \left[1 + \left(\frac{\sigma}{2} \right)^2 \right]^{-1/2} \quad (65)$$

provided that σ be appropriately defined. The form of Eq. (65) was proposed independently by Mellen and Moffett¹³ and by Merklinger¹⁴ as an approximation of the fundamental component taper given by Blackstock.¹⁸ Equation (65) is compared with the Blackstock result in Figure 12, which also shows, for a comparable definition of σ , the taper function derived in Section 3.1. From Figure 12 it appears that the differences among the three functions are not great.

The expressions for σ appropriate for the various authors' treatments of Eq. (65) are now discussed. The Mellen-Moffett¹³ form is given by

$$\sigma = \sigma_0 \sinh^{-1} (r/r_0) \quad (66)$$

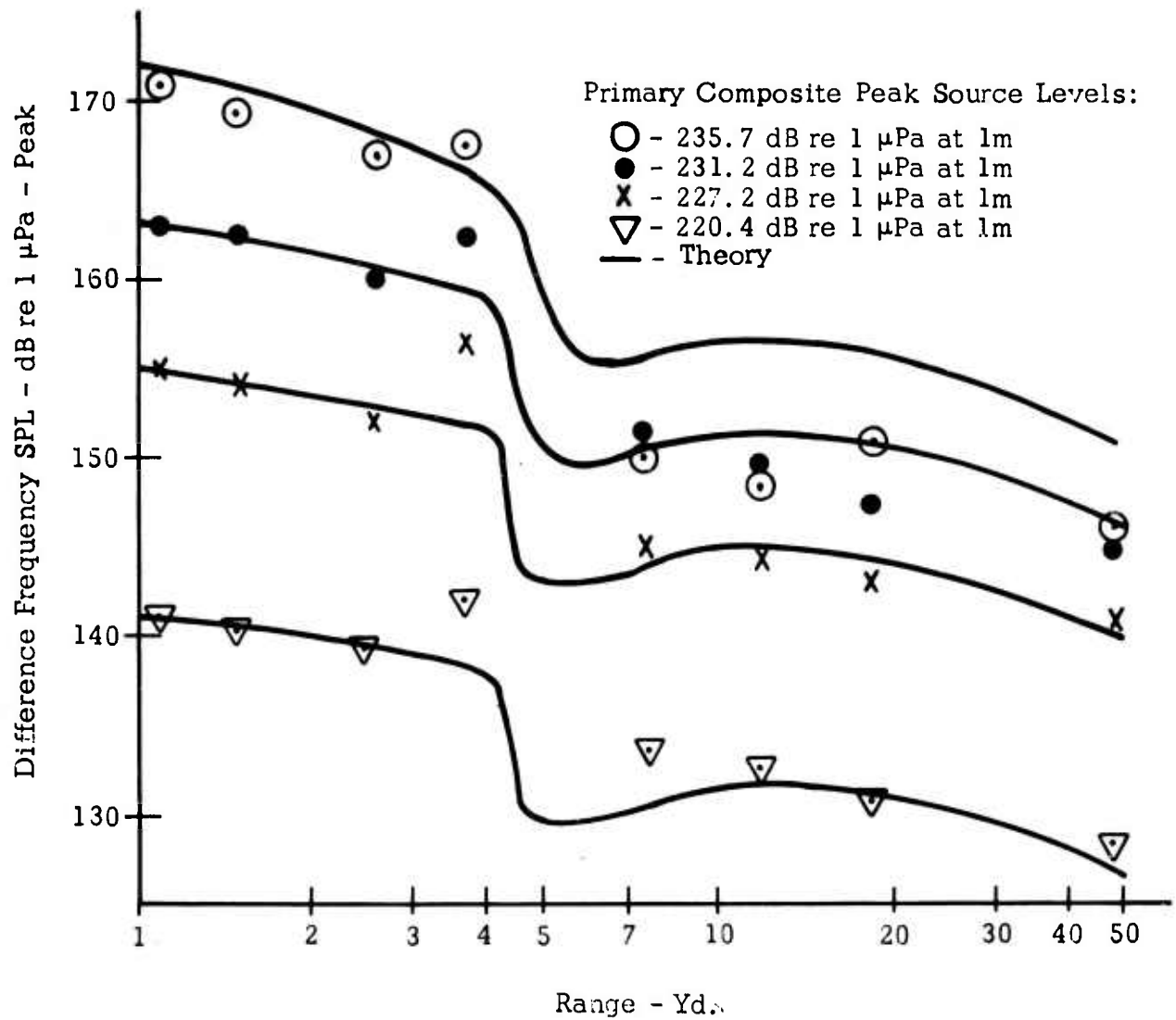


Figure 11. Reflected Parametric Transmitter. Reflector at 4 yd. Difference frequency level data from Mellenbruch & Muir (Ref. 1).

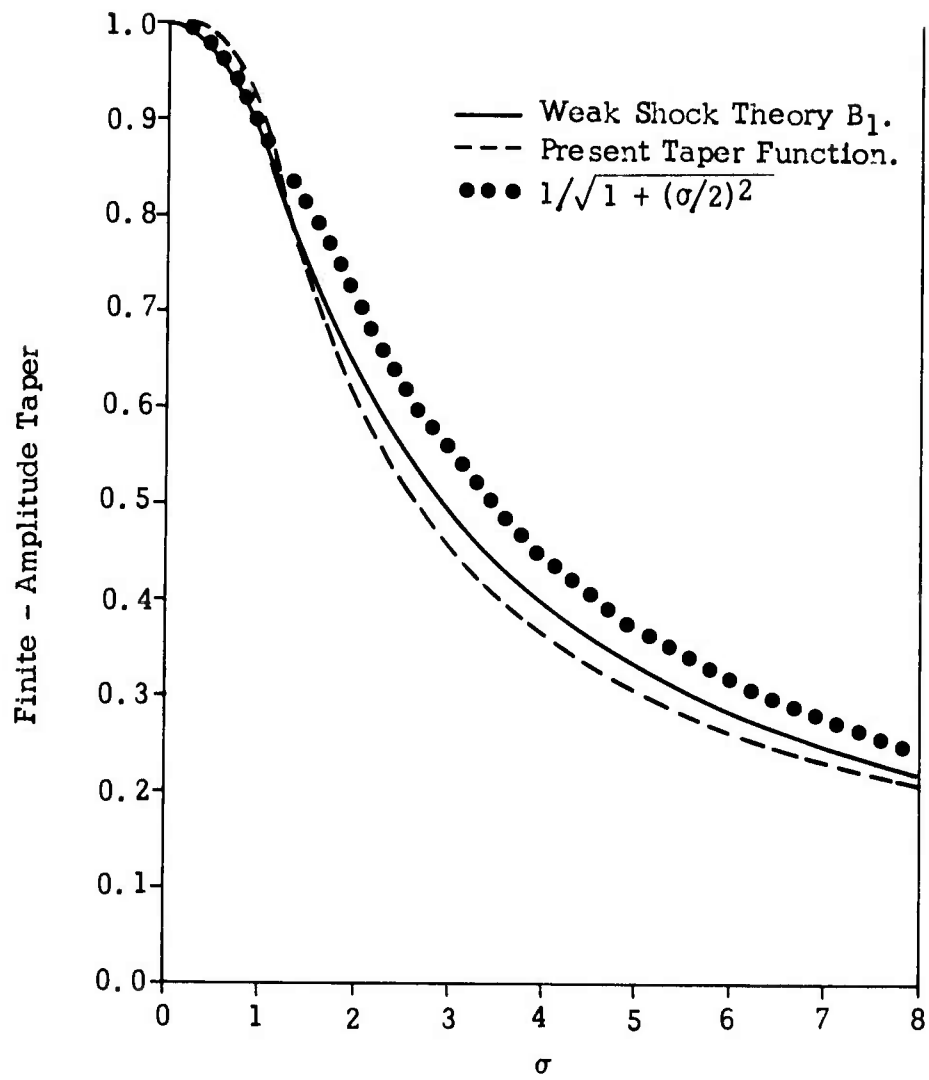


Figure 12. Comparison of Taper Functions with Weak Shock Theory (Ref. 18).

The Merklinger, Mellen and Moffett³³ taper function, hereafter referred to for brevity by the name of the first author only, is given by Eq. (65) with

$$\sigma = \sigma_0 \sqrt{2 e^{\alpha_T r_0} \int_{r_0}^r e^{-4\alpha_0 r'} \frac{dr'}{r'} \int_{r_0}^{r'} e^{2\alpha_0 r''} \frac{dr''}{r''}} . \quad (67)$$

Two taper functions due to Fenlon¹⁶ are the Fenlon Taper Function and the Modified Berkday, Leahy Taper. The appropriate forms of σ are, for Fenlon,

$$\sigma = \sigma_0 \left[E_1(\alpha_T r_0) - E_1(\alpha_T r) \right] e^{\alpha_T r_0} , \quad (68)$$

and for Modified Berkday, Leahy,

$$\sigma = \sigma_0 \left[E_1(\alpha_T r_0) - E_1(\alpha_T r) \right] . \quad (69)$$

Here, $E_1(\cdot)$ represents the exponential integral. Equation (69) is equivalent to the σ used in the taper function derived in Section 3.1 (Eq. 56).

The results of evaluating Eq. (65) as a function of r/r_0 with σ given variously by Eqs. (66), (67), (68), and (69) are shown in Figure 13. This comparison was made for a case when $\alpha_0 r_0$ was small ($\alpha_0 r_0 = .001$). Also, for the Mellen-Moffett calculation the value of r_0 was taken to be twice the value used in the others. It will be seen that there is very little difference between the results of Eqs. (67) and (68). The results of Eq. (69) are so nearly identical to those of Eq. (68) that they have not been shown. The results using Eq. (66) are nearly the same as the others except for small and large values of r/r_0 .

For larger values of $\alpha_0 r$, the disparity among the various forms increases. However, it is likely that the predominant taper will be absorption in cases when there is a significant difference.

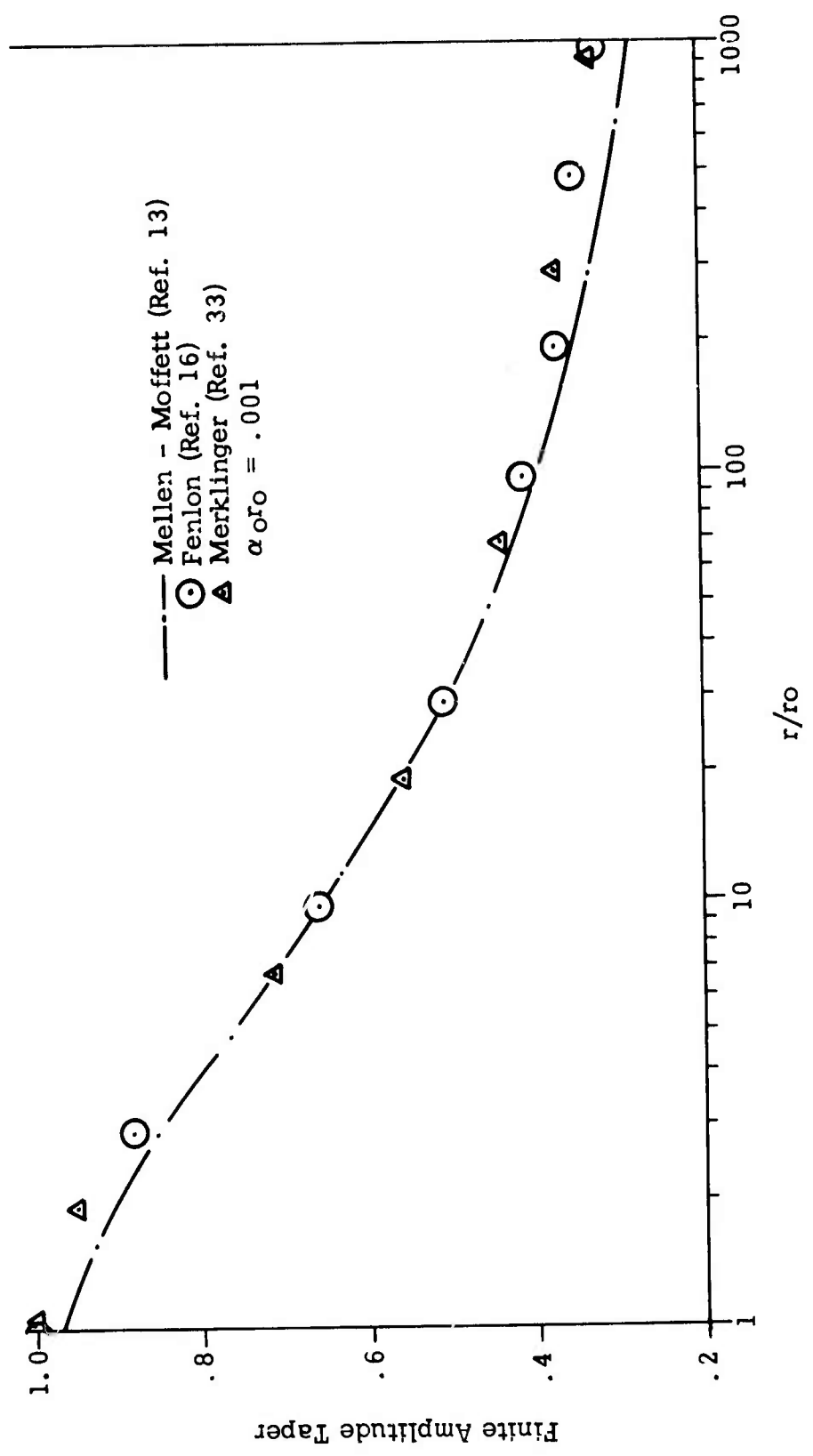


Figure 13. Taper Function Comparison.

3.4 Comparison of Parametric Transmitting Array Calculations Using Various Taper Functions

In the previous section the relative amplitudes of several taper functions were compared. The taper functions considered were identified as the Mellen-Moffett¹³, Fenlon¹⁶, modified Berkday-Leahy¹⁶, Merklinger³³, and intensity taper functions. It was noted that all except the last may be represented by the same function or a single parameter called σ . It is the definition of σ that distinguishes the various tapers. The values of the taper function in the farfield were compared for a particular set of parameters for various theories excluding the intensity taper, and it was concluded that the differences among them were quite small.

The results of using the various tapers in the same numerical volume integration program are now compared. As a basis for comparison we have taken the parametric scaling curves given by Mellen and Moffett. These curves are the solid lines in Figure 14. A single value, 50, of the downshift ratio and a wide range of values for scaled source level and for $(2\alpha R_0)^{-1}$ were chosen. Each taper function except the one derived in the present investigation was defined in two ways; with and without directivity taken into account in defining off-axis values of σ .

The Merklinger and Fenlon σ 's are as defined in the previous report with directivity included by replacing σ_0 by $\sigma_0 D(\theta)$. The modified Berkday-Leahy σ is the same as the expression used in the intensity taper function, which is

$$\sigma = \begin{cases} \sigma_0 \int_0^r e^{-\alpha_T x} dx & r \leq R_0 \\ \sigma_0 \left[\frac{1 - e^{-\alpha_T R_0}}{\alpha_T} + D(\theta) \int_{R_0}^r \frac{e^{-\alpha_T x}}{x} dx \right] & r > R_0 \end{cases} \quad (70)$$

The version without directivity, of course, has $D(\theta) = 1$.

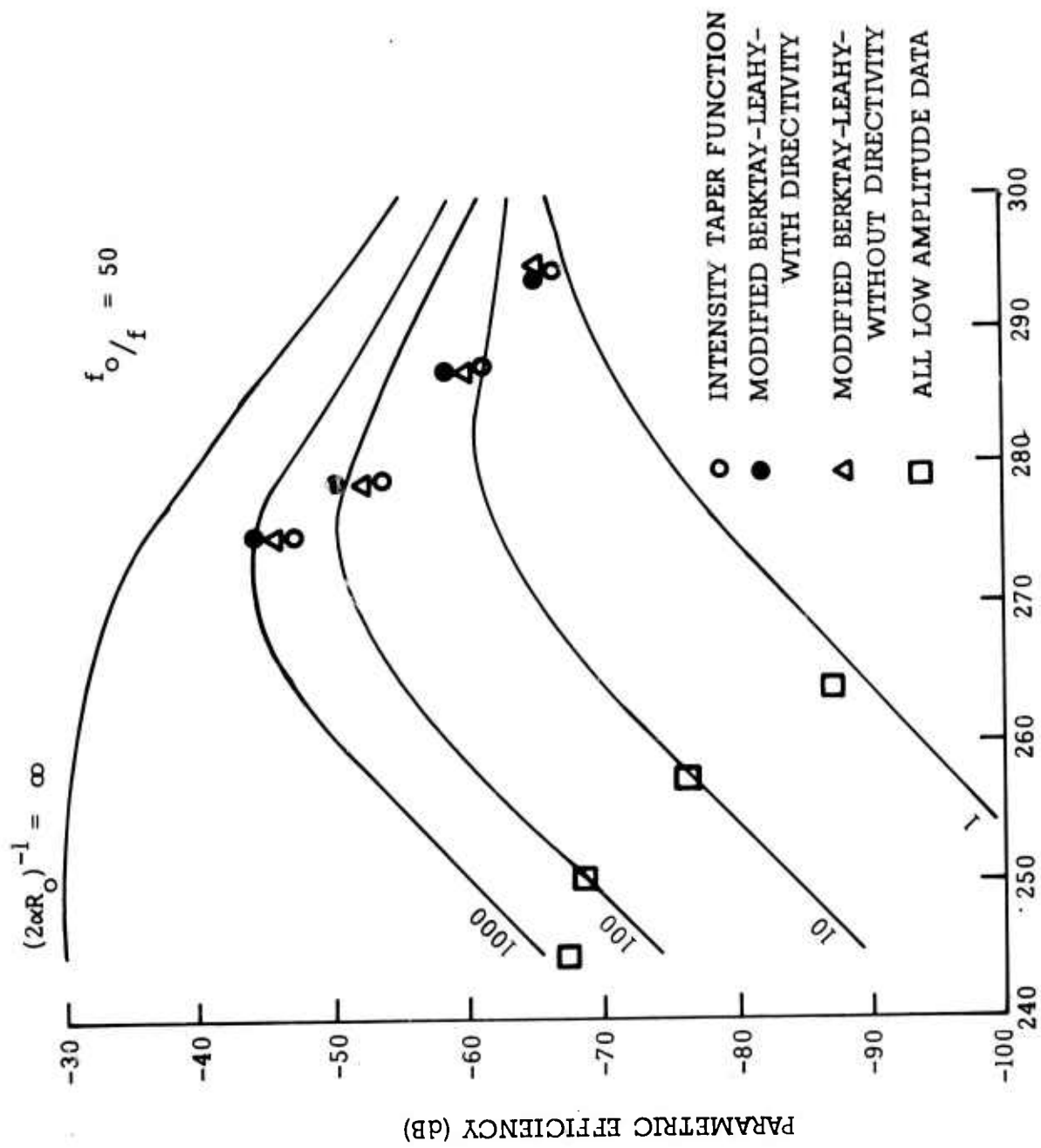


Figure 14. Parametric Efficiency Comparison

As an initial comparison the low amplitude data for $(2\alpha R_0)^{-1} = 1, 10, 100$ and 1000 , are plotted as squares (\square) in Figure 14. For the source level utilized all of the taper functions give the same results. It is interesting that the numerical integration gives virtually identical results to the Mellen-Moffett model at low amplitude, with the exception of the point corresponding to $(2\alpha R_0)^{-1} = 1$, which falls about 3 dB above the solid curve.

The higher amplitude results for the modified Berklay-Leahy and the intensity taper functions are also shown in Figure 14. This comparison demonstrates the difference in results between the two functional forms of the taper theories, with the same σ . A difference of about 3 dB is apparent in each of the cases shown. The modified Berklay-Leahy results without directivity appear about 1.5 dB lower than the results with directivity, except for the nearfield limited case. The results discussed above are all within about 3 dB of the Mellen-Moffett results.

A set of rather surprising results was obtained by using the original Mellen-Moffett taper function in the numerical integration. The calculated parametric efficiencies were within 1 dB of the original model's results. These data are not shown in the figures.

The same data points were run using the Fenlon and the Merklinger taper functions. Unfortunately, the results using these tapers are not directly comparable with those discussed above because they are based on spherical wave theories and do not account for nearfield taper. Their results could have been made to fit the results of other models by appropriate choice of the effective source radius r_0 . The results did indicate that the Fenlon and Merklinger results were within about 1 dB of each other.

It may be concluded that the parametric transmitting array scattering integral is tolerant, with only minor differences in results, of vast differences in approach and in degree of approximation of both geometry and of the taper function. With all of the results lying within 3 dB of each other it would be quite difficult to determine by direct experiment which of the approaches gives the best results. As was noted in the previous section

however, an adaptation of the intensity taper function to the reflected parametric array produced much better results than the present author's earlier adaptation of the Mellen-Moffett theory.

It should be noted that all of the data used in the above comparisons applied to range points well in the farfield of the interaction volume. This condition, which is required for validity of the Mellen-Moffett model, is not necessary in the volume integration approach.

3.5 Conclusions - Parametric Transmitting Array Finite Amplitude Effects

The results reported in Section 3.0 indicate that the simple geometry model proposed by Mellen and Moffett gives results almost identical to those obtained by volume integration, when the same taper function is used. They also demonstrate that accounting for absorption and directivity in defining the taper function associated with nonlinear effects makes very little difference in the results. On the other hand, the manner of describing nonlinear effects in the nearfield and, in spherical wave theories, the choice of the effective source radius r_0 , make substantial differences in the results.

The effects of higher order interactions have not been addressed in the present work. These would be expected to be important only at extremely high intensities.

RECOMMENDATIONS FOR FUTURE WORK

The results of the present investigation point to a clear requirement for additional experimental work. It is unfortunate that the objectives of the experimental portion of this work were not fully realized because of the surprisingly low efficiency of the projectors that were built. These objectives should be pursued further.

A definite requirement exists for concentrating on nearfield saturation effects, both in the parametric receiving array and in the parametric transmitting array. In the case of the parametric receiving array there is a fundamental question yet to be answered regarding the form of the source strength taper in the nearfield. The data presently available suggest that the nearfield and farfield behavior may be distinctly different. The theory presented herein agrees well with farfield data but departs drastically from nearfield data. Additional nearfield data are required to check the one presently available source and to form the basis for a possible composite model that would include both nearfield and farfield effects.

In addition to further investigation of nearfield effects, additional work on the parametric transmitting array should address deriving a taper function that accounts for higher order interactions. Such a taper function would be useful because of the flexibility that the scattering integral approach permits in accurately describing various geometries.

ACKNOWLEDGEMENTS

The author wishes to thank R. Simmons and C. Wyant for transducer fabrication and E. Johnson and R. Simard for their assistance with the experimental work. The technical assistance of the late H. D. Fyffe is also acknowledged.

The cooperation of the Applied Research Laboratories, the University of Texas at Austin is greatly appreciated. Computer programs written by the late J. Willette were supplied by J. Shooter of ARL and were used extensively in the present work. The author is grateful to T. Muir for making available data on the phase reversed parametric array and for an extensive technical correspondence.

The author is especially indebted to W. Konrad, R. Mellen and M. Moffett of the New London Laboratory, Naval Underwater Systems Center for making available revised data and additional unpublished data from their 1971 parametric receiving array experiments. Special thanks to M. Moffett for his efforts in reviewing the aforementioned data and for many helpful discussions and criticisms of our work.

For assistance in preparation of this report, the author thanks J. Lucy who typed the final manuscript and R. Boyd who prepared the graphics. Thanks also to R. Day for his careful review of the draft.

REFERENCES

1. Mellenbruch, L. L. and T. G. Muir, "Experiments on Phase Reversed Shock Propagation and Parametric Generation," J. Acoust. Soc. Am. 55, 429(A) (1974).
2. Westervelt, P. J., "Scattering of Sound by Sound," J. Acoust. Soc. Am. 29, 934 (1957).
3. Westervelt, P. J., "Parametric Acoustic Array," J. Acoust. Soc. Am. 35, 535 (1963).
4. Bellin, J. L. S. and R. T. Beyer, "Scattering of Sound by Sound," J. Acoust. Soc. Am. 32, 339-341 (1960).
5. Berktaf, H. O. and D. J. Leahy, "Farfield Performance of Parametric Transmitters," J. Acoust. Soc. Am. 55, 539 (1974).
6. Fenlon, F. H., "On the Performance of a Dual Frequency Parametric Source via Matched Asymptotic Solutions of Burgers' Equation," J. Acoust. Soc. Am. 55, 35 (1974).
7. Muir, T. G. and J. G. Willette, "Parametric Acoustic Transmitting Arrays," J. Acoust. Soc. Am. 52, 1481 (1972).
8. Berktaf, H. O. and C. A. Al-Temimi, "Virtual Arrays for Underwater Reception," J. Sound Vib. 9, 295 (1969).
9. Konrad, W. L., R. H. Mellen and M. B. Moffett, "Parametric Sonar Receiving Experiments," NUSC Tech. Memo. PA4-304-71 (9 Dec. 1971).
10. Bartram, J. F., "Closed Form Expression for the Source Level of a Finite Amplitude Parametric Array," J. Acoust. Soc. Am. 53, 383(A) (1973).
11. Fenlon, F. H., "An Extension of the Bessel-Fubini Series for a Multiple-Frequency CW Source of Finite Amplitude," J. Acoust. Soc. Am. 51, 284 (1972).
12. Schaffer, M. E. and D. T. Blackstock, "Modulation of a Small-Signal Wave by a Finite-Amplitude Wave of Lower Frequency," J. Acoust. Soc. Am. 57, 573(A) (1975).

13. Mellen, R. H. and M. B. Moffett, "A Model for Parametric and Sonar Radiator Design," NUSC Tech. Memo. PA41-229-71 (1971).
14. Merklinger, H. M., "High Intensity Effects in the Nonlinear Acoustic Parametric Array," PhD thesis, Univ. of Birmingham, Birmingham, England (1971).
15. Bartram, J. F. and P. J. Westervelt, "Nonlinear Attenuation and the Parametric Array," J. Acoust. Soc. Am. 52, 121(A) (1972).
16. Fenlon, F. H., "Approximate Methods for Predicting the Performance of Parametric Sources at High Acoustic Reynolds Numbers," Finite Amplitude Wave Effects in Fluids, L. Bjørnø, Ed., Proc. of the 1973 Symposium, Copenhagen.
17. Fenlon, F. H., "Parametric Scaling Laws," Final Report under Contract N00014-74-C-0214, Westinghouse Res. Labs.
18. Blackstock, D. T., "On Plane, Spherical and Cylindrical Sound Waves of Finite Amplitude in Lossless Fluids," J. Acoust. Soc. Am. 36, 217-219(L) (1964).
19. Blackstock, D. T., "Propagation of Plane Sound Waves of Finite Amplitude in Nondissipative Fluids," J. Acoust. Soc. Am. 34, 9-30 (1962).
20. Fenlon, F. H., "A Recessive Procedure for Computing the Nonlinear Spectral Interactions of Progressive Finite-Amplitude Waves in Nondispersive Fluids," J. Acoust. Soc. Am. 50, 1299 (1971).
21. Merklinger, H. M., H. O. Berktaf and M. H. Safar, "Finite-Amplitude Losses in the Field of Real Transducer," Finite-Amplitude Wave Effects in Fluids, L. Bjørnø, Ed., Proc. of the 1973 Symposium, Copenhagen.
22. Shooter, J. A., T. G. Muir and D. T. Blackstock, "Acoustic Saturation of Spherical Waves in Water," J. Acoust. Soc. Am. 55, 54 (1974).
23. Lockwood, J. C., "Two Problems in High-Intensity Sound. I. Finite Amplitude Sound Propagation in the Farfield of Nonuniform Sources. II. The Diffraction of N Waves by a Circular Aperture in a Plane Baffle," PhD thesis, Mechanical and Aerospace Sciences Dept., Univ. of Rochester (July 1971). Also issued as ARL Tech. Report No. 71-26 (ARL-TR-71-26) (July 1971) (AD 740-498).

24. Lockwood, J. C. , "Approximate Time Domain Solution for Finite Amplitude Spherical Waves in an Absorbing Medium," Finite Amplitude Wave Effects in Fluids, L. Bjørnø, Ed. , Proc. of the 1973 Symposium, Copenhagen.
25. Lockwood, J. C. , T. G. Muir and D. T. Blackstock, "Directive Harmonic Generation in the Radiation Field of a Circular Piston," J. Acoust. Soc. Am. 53, 1148-1152 (1973).
26. Browning, D. G. and R. H. Mellen, "Finite-Amplitude Distortion of 150 kHz Acoustic Waves in Water," J. Acoust. Soc. Am. 44, 644(L) (1968).
27. Muir, T. G. and J. E. Blue, "Experiments on the Acoustic Modulation of Large Amplitude Waves," J. Acoust. Soc. Am. 46, 227 (1969).
28. Lockwood, J. C. , "Theoretical Performance of a Parametric Array with Phase-Reversed Primary Radiation," J. Acoust. Soc. Am. 55, 429(A) (1974).
29. Lockwood, J. C. , "Investigation of Finite Amplitude Attenuation, Quarterly Technical Report No. 1," under Contract N00039-75-C-0263, ARPA Order 2910, Program Code 5G10, AMETEK, Straza Div. , El Cajon, Ca. 92020 (June 1975).
30. Berklay, H. O. and J. A. Shooter, "Parametric Receivers with Spherically Spreading Pump Waves," J. Acoust. Soc. Am. 54, 1056 (1973).
31. Lockwood, J. C. and D. P. Smith, "Investigation of the Increase in Parametric Efficiency due to Bubbles," AMETEK, Straza Div. Tech. Report. No. 11-1354E-74-1 (1974).
32. Moffett, B. M. , Private Communication (Jan. 1976).
33. Merklinger, H. M. , R. H. Mellen and M. B. Moffett, "Finite-Amplitude Losses in Spherical Sound Waves," J. Acoust. Soc. Am. 53, 383(A) (1973).
34. Barnard, G. R. , J. G. Willette, J. J. Truchard and J. A. Shooter, "Parametric Receiving Array," J. Acoust. Soc. Am. 52, 1437 (1972).
35. Berklay, H. O. and T. G. Muir, "Arrays of Parametric Receiving Arrays," J. Acoust. Soc. Am. 53, 1377 (1973).

36. Berkday, H. O. , "Parametric Amplification by the Use of Acoustic Non-linearities and Some Possible Applications," J. Sound Vib. 2, 462 (1965).
37. Berkday, H. O. , "Possible Exploitation of Nonlinear Acoustics in Underwater Transmitting Applications," J. Sound Vib. 2, 435 (1965).
38. Truchard, J. J. , "A Theoretical and Experimental Investigation of the Parametric Acoustic Receiving Array," ARL Tech. Report No. 74-17 (1974).
39. Moffett, M. B. , "Parametric Radiation Theory," NUSC Tech. Memo No. PA4-234-71 (1971).
40. Berkday, H. O. and C.A. Al-Temimi, "Scattering of Sound by Sound," J. Acoust. Soc. Am. 50, 181 (1969).
41. Berkday, H. O. and J. A. Shooter, "Nearfield Effects in End-Fire Line Arrays," J. Acoust. Soc. Am. 53, 550 (1973).

DISTRIBUTION LIST

Copy No.

- 1
Commander
Naval Electronic Systems Command
Department of the Navy
Washington, DC 20362
Attn: Code 3204
- 2
Commander
Naval Electronic Systems Command
Department of the Navy
Washington, DC 20362
Attn: Code 2703
- 3-4
Commander
Naval Electronic Systems Command
Department of the Navy
Washington, DC 20362
Attn: Dr. Joel Sinsky, Code 320
- 5-6
Defense Advanced Research Projects Agency
1400 Wilson Blvd.
Arlington, VA 22209
Attn: CDR W. Jordan (TTO)
- 7
Director
Naval Research Laboratory
Department of the Navy
Washington, DC 20375
Attn: Code 8150
- 8
Director
Naval Research Laboratory
Department of the Navy
Washington, DC 20375
Attn: Code 8151
- 9
Officer-in-Charge
New London Laboratory
Naval Underwater Systems Center
Department of the Navy
New London, CT 06320
Attn: M. B. Moffett (Code TD 124)
- 10
Officer-in-Charge
New London Laboratory
Naval Underwater Systems Center
Department of the Navy
New London, CT 06320
Attn: W. Konrad

Copy No.

- 11 Battelle Memorial Institute
505 King Avenue
Columbus, OH 43201
Attn: TACTEC
- 12-13 Defense Documentation Center
Defence Services Administration
Cameron Station, Building 5
5010 Duke Street
Alexandria, Virginia 22314
- 14 Westinghouse Electric Corporation
Defense and Electronic Systems Center
Baltimore-Washington International Airport
P. O. Box 1693
Baltimore, MD 21203
Attn: A. Nelkin, Annapolis Branch
- 15 Chief of Naval Research
Department of the Navy
Arlington, VA 22217
Attn: Code 222
- 16 Chief of Naval Research
Department of the Navy
Arlington, VA 22217
Attn: Code 212
- 17 Commander
Naval Undersea Center
San Diego, California 92132
Attn: Library (J. Reeves/L. Frandsdal)
- 18 Superintendent
Naval Postgraduate School
Monterey, CA 93940
Attn: Technical Library (H. Medwin)
- 19 Superintendent
Underwater Sound Reference Division
P. O. Box 8337
Orlando, FL 32806
Attn: Dr. Joe Blue
- 20 Department of Electronic & Electrical Engineering
University of Birmingham
P. O. Box 363
Birmingham B15 2TT, ENGLAND
Attn: Professor H. O. Berkday
- 21 Department of Physics
Chelsea College
London, ENGLAND
Attn: Dr. R. W. B. Stephens

Copy No.

- 22 Fluid Mechanics Department
The Technical University of Denmark
Building 404
DK-2800 Lyngby, DENMARK
Attn: Dr. L. Bjørnø
- 23 Physics Institute
University of Bergen
5014 Bergen-U
NORWAY
Attn: Dr. M. Vestrheim
- 24 Defense Research Establishment Atlantic
P. O. Box 1012
Dartmouth, Nova Scotia
CANADA
Attn: H. M. Merklinger
- 25 Department of Physics
Brown University
Providence, RI 02912
Attn: Professor R. T. Beyer
- 26 Department of Physics
Brown University
Providence, RI 02912
Attn: Professor P. J. Westervelt
- 27 Department of Physics
Brown University
Providence, RI 02912
Attn: Professor A. O. Williams, Jr.
- 28 Department of Physics
Kalamazoo College
Kalamazoo, MI 49001
Attn: Professor W. M. Wright
- 29 Applied Research Laboratories
The University of Texas at Austin
P. O. Box 8029
Austin, Texas 78712
Attn: G. Barnard
- 30 Applied Research Laboratories
The University of Texas at Austin
P. O. Box 8029
Austin, Texas 78712
Attn: T. Goldsberry

Copy No.

- 31 Applied Research Laboratories
The University of Texas at Austin
P. O. Box 8029
Austin, Texas 78712
Attn: J. Clynych
- 32 Applied Research Laboratories
The University of Texas at Austin
P. O. Box 8029
Austin, Texas 78712
Attn: T. Muir
- 33 Applied Research Laboratories
The University of Texas at Austin
P. O. Box 8029
Austin, Texas 78712
Attn: D. Blackstock
- 34 Applied Research Laboratories
The University of Texas at Austin
P. O. Box 8029
Austin, Texas 78712
Attn: J. Shooter
- 35 Raytheon Company
Submarine Signal Division
P. O. Box 360
Portsmouth, R.I. 02871
Attn: J. Bartram
- 36 Raytheon Company
Submarine Signal Division
P. O. Box 360
Portsmouth, R.I. 02871
Attn: G. Walsh
- 37 Raytheon Company
Submarine Signal Division
P. O. Box 360
Portsmouth, R.I. 02871
Attn: R. Pridham
- 38-42 Raytheon Company
Submarine Signal Division
P. O. Box 360
Portsmouth, R.I. 02871
Attn: J. Lockwood

Copy No.

43	Applied Research Laboratory Pennsylvania State University State College, PA 16801 Attn: F. Fenlon
44	G. Brigham
45	R. Day
46	D. Hollman
47	R. Simmons
48	AMETEK, Straza Division Library
49-50	Reserve Copies

REPORT DOCUMENTATION PAGE		READ INSTRUCTIONS BEFORE COMPLETING FORM
1. REPORT NUMBER	2. GOVT ACCESSION NO.	3. RECIPIENT'S CATALOG NUMBER
6. TITLE (and Subtitle) INVESTIGATION OF FINITE AMPLITUDE ATTENUATION,		9. TYPE OF REPORT & PERIOD COVERED Final Technical Report. 29 Mar. -31 Dec. 1975
7. AUTHOR(s) James C. Lockwood		14. PERFORMING ORG. REPORT NUMBER 11-1554E-76-6
9. PERFORMING ORGANIZATION NAME AND ADDRESS AMETEK, Straza Division 790 Greenfield Drive El Cajon, Calif. 92022		15. CONTRACT OR GRANT NUMBER(s) N00039-75-C-0263
11. CONTROLLING OFFICE NAME AND ADDRESS Defense Advanced Research Projects Agency 1400 Wilson Blvd., Arlington, Va. 22209		10. PROGRAM ELEMENT, PROJECT, TASK AREA & WORK UNIT NUMBERS Program Code 5G10 ARPA Order-2910
14. MONITORING AGENCY NAME & ADDRESS (if different from Controlling Office) Naval Electronic Systems Command Washington, D. C.		12. REPORT DATE 29 Feb. 1976
		13. NUMBER OF PAGES 60
		15. SECURITY CLASS. (of this report) UNCLASSIFIED
		15a. DECLASSIFICATION/DOWNGRADING SCHEDULE
16. DISTRIBUTION STATEMENT (of this Report) Approved for Public Release; Distribution Unlimited.		
17. DISTRIBUTION STATEMENT (of the abstract entered in Block 20, if different from Report)		
18. SUPPLEMENTARY NOTES		
19. KEY WORDS (Continue on reverse side if necessary and identify by block number) Nonlinear Acoustics Parametric Receiving Array Parametric Transmitting Array Saturation		
20. ABSTRACT (Continue on reverse side if necessary and identify by block number) This is the final technical report on a study of finite amplitude attenuation that has been performed under Contract N00039-75-C-0263, Program Code 5G10, ARPA Order 2910. The program objective has been to determine by experimental and theoretical means the limitations imposed by finite amplitude attenuation on the performance of parametric sonars. The results are intended for use in assessing the potential of parametric receivers and transmitters in military applications.		

388 891 ✓

410

20. ABSTRACT

The axial response of the parametric receiving array has been calculated in two ways. The first is by use of a one dimensional model in which the secondary signal levels are predicted from weak shock theory. The second is by numerical evaluation of the scattering integral solution in which finite amplitude attenuation is introduced by means of a taper function derived from the one dimensional solution.

An experiment has been performed in which the axial secondary signal level as a function of pump source level was measured. These data agree with the theoretical results, but the agreement is not conclusive because the maximum pump source level was not sufficiently high. However, a comparison with data from another investigation confirms the theory for cases when the receiving hydrophone is well in the farfield of the pump.

Comparison with a set of experimental results for which the interaction was almost entirely in the pump nearfield indicates that, unlike the farfield case, the nearfield behavior may be quite different from that predicted by the present theory. Caution is therefore advised in applying the present results to near-field interactions.

In addition to the parametric receiving array work, several parametric transmitting array taper functions have been compared in the context of numerical evaluations of the scattering integral. A mean taper function is derived from weak shock theory and is compared with the others.

In all cases the results are surprisingly similar to those obtained using the model given by Mellen and Moffett.